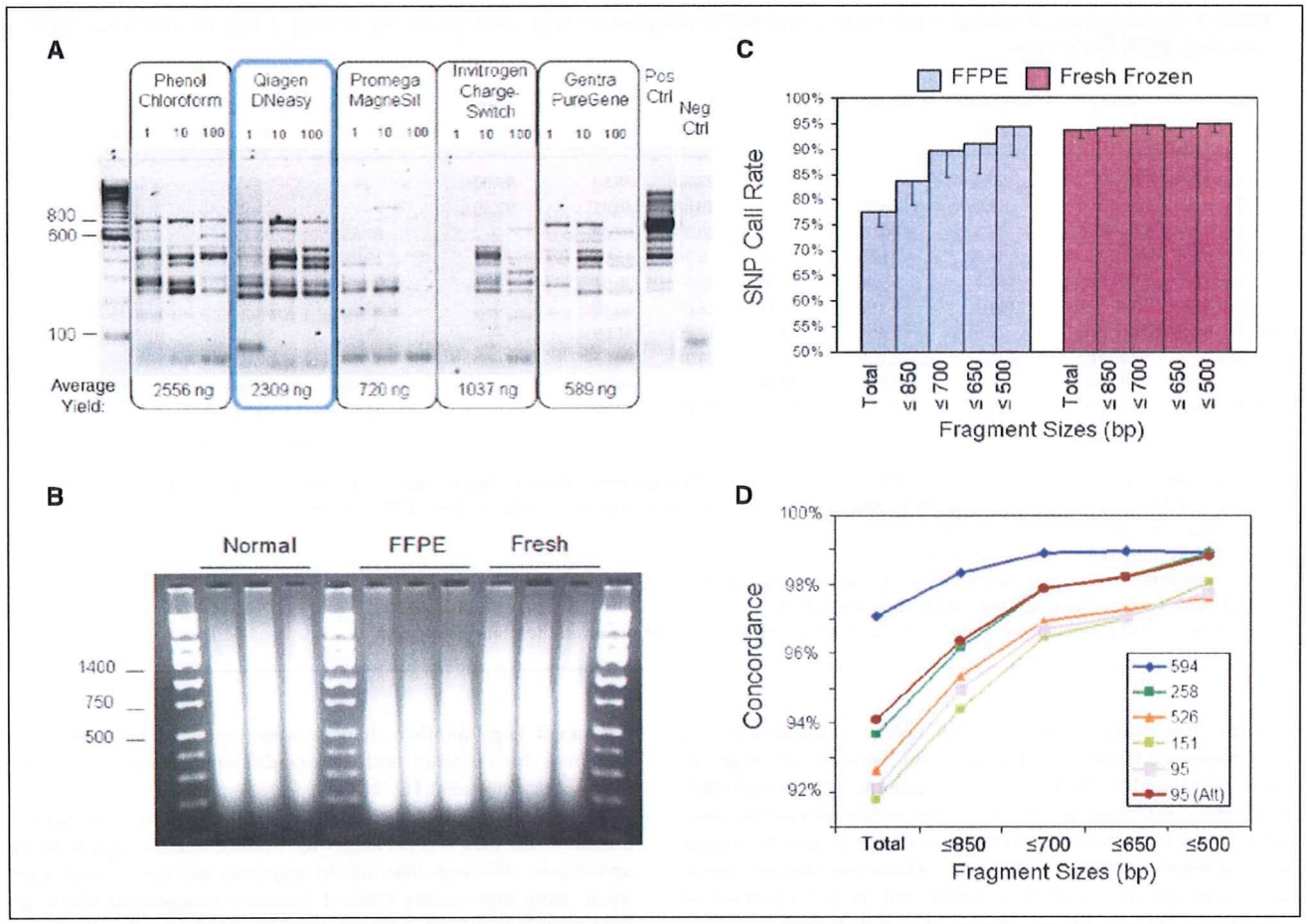

Figure 1. Performance of different FFPE DNA extraction methods and the Affymetrix GeneChip Mapping 500K assay. *A*, visualization of RAPD-PCR products on a 3% agarose gel comparing the undiluted DNA extraction (1), a 1:10 dilution of input DNA (10), and a 1:100 dilution of DNA (100) from one FFPE tissue (047) using five different extraction methods. The maximum fragment size in the extracted FFPE DNA samples reached 1,100 bp although only with sample dilution. The maximum reproducible fragment was 800 bp. DNA yield per extraction method is listed below. *B*, visualization of the PCR products during the Mapping 500K assay reveals a downshift in the distribution of fragment size, which is specific to the FFPE samples. *C*, SNP call rates are reduced in FFPE samples, but SNPs on smaller fragments are genotyped with equal efficiency from fresh and paraffin samples. The size dependence for higher call rates is specific to the FFPE samples. *D*, concordance between fresh frozen and matching FFPE samples is incrementally increased with fragment size selectivity, with larger dips in accuracy for sizes >700 bp. Exclusion of some regions (chromosomes 1q, 7p, 15, and 16q) shown to be genetically different between 95 fresh and FFPE samples causes an upshift in concordance for this sample (95 Alt versus 95).

63 to 83 μg PCR products for the Mapping 250K Nsp Array, whereas all non-FFPE samples produced >90 μg.

The assay was continued using 90 μg PCR product as the manual instructs or the total PCR yield when this was less than assay requirements. Importantly, the protocol was otherwise never modified. Normal and fresh tumor samples gave typical SNP call rates, with an average of 94.5% and 93.5%, respectively. These call rates are lowered due to application of a strict confidence score threshold ($P \leq 0.26$; the default threshold is $P \leq 0.33$). In contrast, FFPE samples achieved an overall average call rate of 79.84% and 75.17% for Nsp and Sty, respectively (Table 1). These decreased call rates are consistent with the poor amplification of larger fragments during PCR. Exclusion of SNPs on larger fragments significantly increased the call rates, such that incrementally more stringent fragment size restrictions incrementally increased call rates (Fig. 1*C*). In fact, stringent fragment size restrictions produced similar call rates between fresh frozen and FFPE samples, indicating that the Mapping 500K is well suited for FFPE DNA and identifying the limiting factor as the size of amplicons produced from the degraded DNA.

Concordance of genotype calls between paired FFPE and fresh frozen ovarian tumor DNA samples was examined to determine the reliability of genotypes from FFPE DNA. It is important to note that tumor heterogeneity lead to confirmed genuine differences in genomic content between matched FFPE and fresh frozen DNA, which would lower these concordance rates. Average overall concordance between FFPE and fresh frozen samples from the same tumor was 93.6%. Exclusion of the larger fragments increased concordance such that all SNPs located on fragment sizes ≤700 bp displayed an average of 97.4% concordance (Fig. 1*D*). Exclusion of several regions (chromosomes 1q, 7p, 15, and 16q) displaying heterogeneity between fresh frozen and paraffin sample 95 increased the concordance by >2% (Fig. 1*D*). These high rates of concordance, despite shown genetic differences between paired samples, underscore the reliability and reproducibility of genotype calls produced using FFPE-derived DNA samples with this

Table 1. Performance of normal, fresh frozen, and FFPE samples on Affymetrix GeneChip Mapping 10K v2, 50K Xba, 250K Nsp, and 250K Sty arrays

Type	Array	PCR yield* (μg)	Call rate† (%)	AA call (%)	AB call (%)	BB call (%)	Signal detection‡ (%)	MCR§ (%)	MDR‖ (%)	Overall concordance¶ (%)
Fresh tumor	10K v2	20.4	93.44	37.96	23.50	38.54	99.82	—	—	96.20
FFPE tumor	10K v2	19.2	86.30	39.77	19.83	40.41	97.39	—	—	
Fresh tumor	50K Xba	48.3	90.07	40.28	20.24	39.48	—	87.65	98.57	56.95
FFPE tumor	50K Xba	46.0	31.86	47.30	6.76	45.94	—	15.25	22.15	
Normal	250K Nsp	115.1	95.86	37.95	25.54	36.51	—	94.22	98.60	
Fresh tumor	250K Nsp	114.4	93.99	41.81	18.09	40.10	—	88.26	98.52	94.74
FFPE tumor	250K Nsp	71.6	79.84	43.42	14.89	41.69	—	65.60	80.32	
Normal	250K Sty	121.1	93.05	38.87	24.28	36.85	—	90.90	97.45	
Fresh tumor	250K Sty	114.4	92.96	42.38	17.59	40.03	—	87.95	98.38	92.07
FFPE tumor	250K Sty	95.4	75.17	43.66	16.68	39.66	—	62.57	79.37	

*For the 250K arrays, this is the total yield of DNA obtained after combining three PCRs according to protocol. For the 10K v2 and 50K arrays, the PCR yield for the FFPE tissues was increased by increasing either the number of reactions or the number of PCR cycles.
† Percentage of SNPs able to be genotyped.
‡ Signal detection used to assess 10K arrays.
§Modified partitioning around medoids (MPAM; a genotyping algorithm; ref. 17) call rate used to assess 100K and 500K arrays.
‖MPAM detection rate used to assess 100K and 500K arrays.
¶Percentage of SNPs genotyped in both fresh frozen and FFPE samples that are given the same genotype.

platform. Importantly, it indicates the need to exclude SNPs on larger fragments for reliable genotype data. Because SNP fragment size is distributed randomly across the genome, the general effect of excluding larger fragment sizes is to reduce the overall resolution without preferentially losing extensive coverage in specific regions (see Supplementary Fig. S1). The effect of fragment size on concordance was specific to FFPE samples and is not observed in comparisons between frozen samples (data not shown).

LOH and copy number assessment. The reliability of genotype assignments using paraffin samples suggests their suitability for LOH predictions. In fact, FFPE and fresh tumor pairs produced similar LOH profiles when including SNPs on fragments sizes ≤700 bp (Fig. 2*A*). Regions of inconsistent LOH predictions between paired samples (for example, see Fig. 2*A*, *boxes*) were predicted independently by both Nsp and Sty arrays and appeared along concentrated regions, rather than being sporadically distributed across the genome, suggesting that they reflected true biological differences between the samples. We assessed several discordant regions of LOH using conventional microsatellite marker analysis and in all cases, the microsatellite analysis confirmed that the array predictions were genuine (data not shown).

The ability to associate copy number estimates with SNP genotypes relies on quantitation of SNP probe intensities (14). Because larger fragment SNPs were inadequately amplified during WGSA, these SNPs were noninformative for copy number analysis of FFPE samples (Supplementary Fig. S2A). Exclusion of these large fragment SNPs significantly increased the amplitude (signal) of copy number shifts and at the same time reduced the SD (noise) associated with the copy number estimates for all FFPE samples but not the fresh frozen samples (Supplementary Fig. S2B). This increase in signal to noise ratio justifies the use of such a filter, which maintained 308,788 SNPs for FFPE copy number analysis (Table 2). Probe intensities from the remaining smaller fragment SNPs predicted copy number profiles for FFPE samples consistent with those from matching fresh frozen material (Fig. 2*B*). Equivalent copy number changes were predicted between FFPE and fresh frozen pairs both across different chromosomes and different sample sets (Fig. 2*C*).

In addition to limiting fragment size, compensation against fragment size bias was necessary to produce reliable copy number predictions. Although bias due to amplicon size can be negligible when using high-quality DNA, it becomes exaggerated when the DNA sample is degraded (Fig. 3, *top*). For FFPE samples, the mean copy number was grossly affected by the size of the amplicon carrying the SNP, such that smaller amplicons SNPs predicted gains and larger amplicons SNPs predicted losses in copy number. Quadratic regression helped to neutralize this fluctuation in mean copy number (Fig. 3, *middle*). Exclusion of SNPs on amplicons >700 bp before regression effectively removed the fragment size bias from copy number detection (Fig. 3, *bottom*). Copy number analysis of FFPE samples was done using the freely available CNAG_v2.0 software[12] (15), which automatically uses compensation against fragment size bias and includes an option to exclude SNPs based on fragment size. Alternate software tools that lack this compensation produced copy number estimates from FFPE samples that were noisier even with exclusion of large fragment sizes (data not shown).

Comparison of Mapping 10K, 100K, and 500K array performance. Although the various Mapping arrays all use the same technology and similar assays for genotype and copy number analysis, they each have differences that may influence their compatibility with FFPE samples. Particularly, the Mapping 500K and 10K arrays share the same amplicon distribution during the PCR step of WGSA, but the Mapping 100K assay relies on a wider amplicon size distribution (250–2,000 bp). Consequently, Mapping 100K data are more significantly affected by DNA degradation; for example, there are only 59 SNPs on fragment sizes <500 bp on the Mapping 50K Hind array. Previously, we showed the application of FFPE DNA to the 10K arrays (3) although without the analytic tools applied here. Now, we compared performance of FFPE samples on all Mapping arrays. As expected, call rates and concordances were

poor when FFPE DNA was applied to the Mapping 100K assay, whereas performance was similar for the Mapping 500K and 10K arrays (Table 1; Supplementary Fig. S3). Furthermore, both the Mapping 500K and the 10K arrays, but not the Mapping 100K arrays, provided correct copy number predictions from FFPE DNA, whereas the Mapping 500K arrays best accommodated SNP filters to retain high genomic resolution (Supplementary Fig. S3).

Prediction of mapping array performance for a range of FFPE samples. DNA from FFPE samples can vary in quality as a result of the fixation protocol, years of storage, the extraction protocol, tissue source, and several other uncontrollable and controllable variables. To both identify a method for qualifying FFPE DNA samples for array analysis and test our guidelines for FFPE DNA extraction and data analysis, we measured the performance of an additional 25 FFPE tissue sources processed at separate institutes and stored for 1 to 17 years (Supplementary Table S1). These samples were not prescreened nor selected based on expected performance. Experiments were done without matched fresh frozen or nontumor samples. In a small test set, we found that application of 90 μg PCR product from FFPE samples increased call rates by several percentage points (data not shown); therefore, we assayed these samples using 90 μg whenever possible, even if this required pooling extra PCRs.

For each sample, we noted the largest amplicon size produced during RAPD-PCR as well as the size range of PCR products during the Mapping assay. Call rates were calculated for SNPs on fragment size ≤200 bp, 250 bp, 300 bp, and so on to determine the size at which call rates dropped <90%. This call rate drop-off value was used to indicate genotyping efficiency and reliability because fragment sizes with high call rates provided high concordance as well. Call rate drop-off values ranged from 250 to 750 bp compared with 700 to 850 bp for the five FFPE ovarian tumors. Therefore, most of these samples would provide reduced resolution for genotype and LOH. Copy number detection was more robust than genotype, and those cutoffs ranged from 300 bp up to no filter requirement at all. Plots of copy number versus fragment size were evaluated to

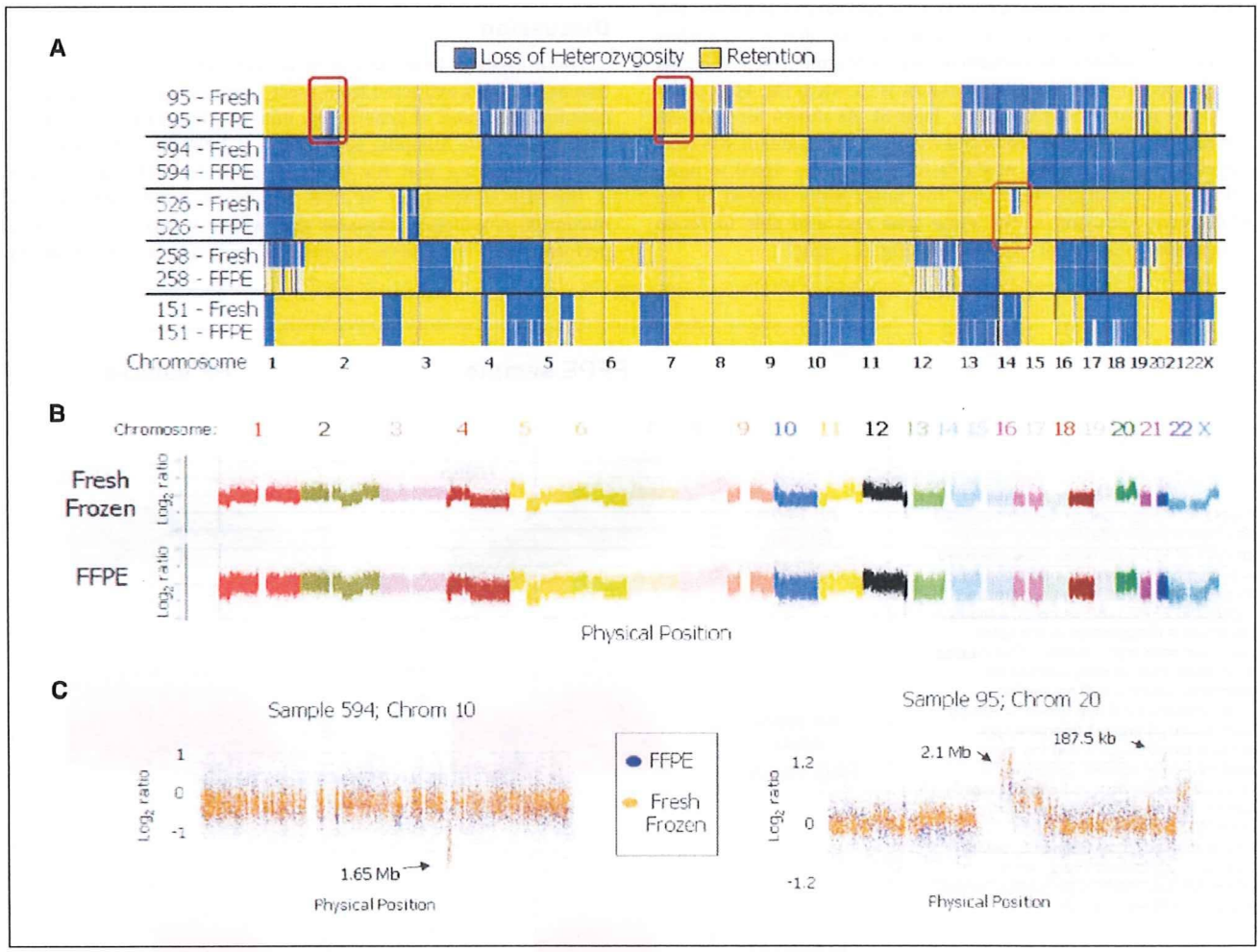

Figure 2. Genome-wide plots of LOH and copy number for fresh frozen and FFPE samples. *A*, genome-wide display of inferred LOH for fresh frozen and FFPE samples, including SNPs on fragments sizes ≤700 bp. *Blue regions*, LOH; *yellow regions*, retention of heterozygosity. Chromosome numbers are indicated below. Three discordant LOH predictions specific to either fresh frozen or FFPE samples were confirmed by microsatellite analysis of DNA (*brown boxes*, regions). *B*, raw single SNP log 2 ratios indicate gains and losses for fresh frozen (above) and FFPE (below) sources of sample 151 across the genome. Ratios represent copy number of tumor DNA over copy number of nontumor, non-FFPE lymphocytic DNA. Each color represents a different chromosome. SNPs were filtered for fragments ≤700 bp for the FFPE sample. *C*, raw single SNP log 2 ratios for fresh frozen (*orange*) and FFPE (*blue*) DNA are plotted across single chromosomes of multiple samples. SNPs were filtered for fragments ≤700 bp for FFPE data only. Highlighted copy number changes were confirmed by quantitative PCR.

Table 2. SNP numbers per fragment size filters

Fragment sizes included (bp)	250K Nsp array	250K Sty array	500K array set
≤300	13,636	15,845	29,481
≤400	39,492	45,473	84,965
≤500	74,372	82,099	156,471
≤600	113,687	120,025	233,712
≤650	133,748	138,282	272,030
≤700	153,198	155,590	308,788
≤800	190,899	187,687	378,586
≤850	209,017	201,004	410,021
≤900	222,316	213,300	435,616
≤1,000	244,644	230,527	475,171
Total	262,256	238,300	500,568

determine the optimal fragment size filter for copy number analysis. These plots can be viewed in CNAG_v2.0, and various fragment size filters can be applied until the mean copy number for the SNPs retained in analysis are consistent across fragment size (Fig. 4*C*, *left*). An example of this entire workflow is shown in Fig. 4*A* to *C* and results are listed in Supplementary Table S1. As shown for a 733-kb hemizygous loss highlighted in this example, the fragment size filter suggested by this process was able to increase the signal to noise ratio by preferentially removing the noisy SNPs instead of the informative SNPs and at the same time was also able to retain higher resolution by not overfiltering (Fig. 4*C*, *right*).

Years of storage and overall call rates displayed some correlation to copy number and call rate drop-off values, but PCR-based analyses had higher predictive power for these performance metrics (Fig. 4*D*). The Pearson's correlation of median RAPD-PCR values to copy number drop-off was 0.93, indicating high predictive power. Comparison of array performance to PCR-based DNA quality tests gave R^2 values above 0.8. In contrast, R^2 values were <0.7 when comparing performance with years of storage or comparing copy number drop-off with overall call rate. These results indicate that a PCR-based test of DNA quality is a reasonable method for predicting whether a FFPE DNA sample will be amenable to array analysis.

Six of the 25 samples (two breast and four colorectal) were not applied to the arrays because no RAPD-PCR products were produced. Sample 0588 also failed RAPD-PCR, but it was still applied to the array. Consistent with the RAPD-PCR prediction, this sample was the only example, in which call rates broken up by fragment size never exceeded 90%, and data from even the smallest fragment SNPs were too noisy for copy number analysis.

Discussion

There exists a large and growing deposit of archived clinical tissues, yet DNA extracted from these samples is usually degraded, contaminated, and of general low quality. This study expands the usefulness of the Mapping 500K arrays to DNA derived from FFPE samples, showing that the limiting factor for FFPE application is the size distribution of PCR amplicons during WGSA. The maximum amplifiable fragment size, which is correlated to array performance, varied between samples and may be influenced by

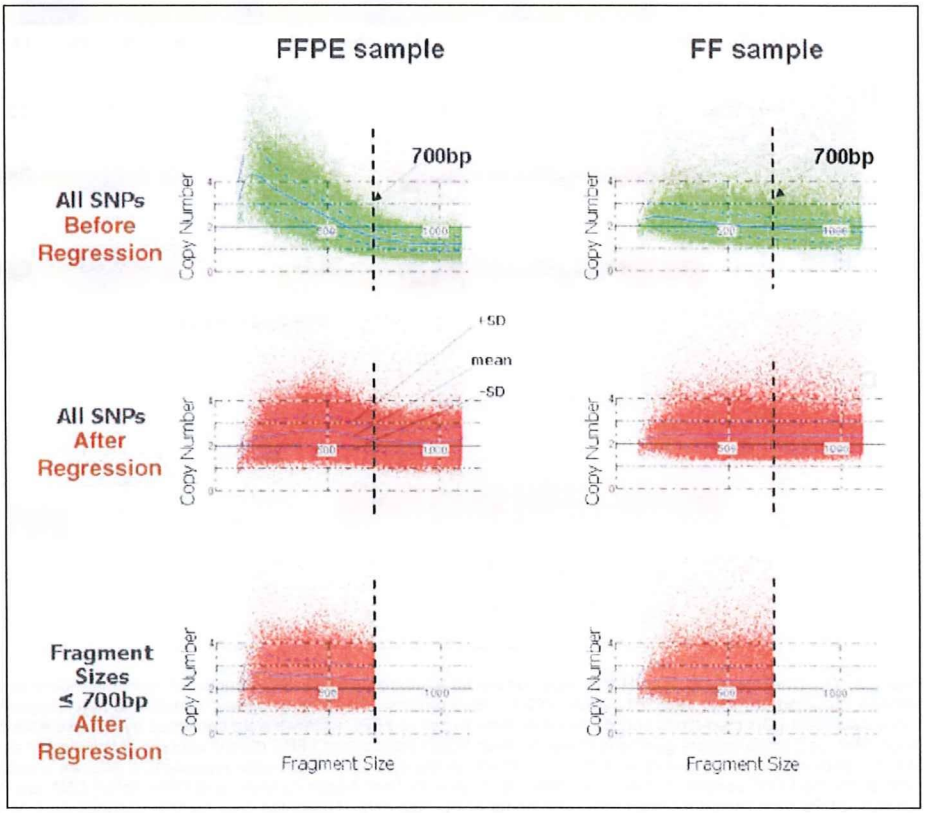

Figure 3. Compensation against fragment size bias enables effective copy number analysis of FFPE samples. Raw predicted copy number (*Y-axes*) is influenced by fragment size (*X-axes*) in fresh frozen (*right*) and FFPE (*left*) samples, although the effect is exaggerated in the latter (see *blue solid lines, middle*). This causes an overestimate of copy number for fragments below ~500 bp and an underestimate for those above ~500 bp. Compensation against fragment size corrects this bias such that the mean predicted copy number (*blue line*) is constant independent of fragment size in fresh frozen samples (*bottom right*). For FFPE samples, exclusion of noninformative larger fragments before quadratic regression is required to effectively equilibrate copy number across maintained SNPs (*top left*).

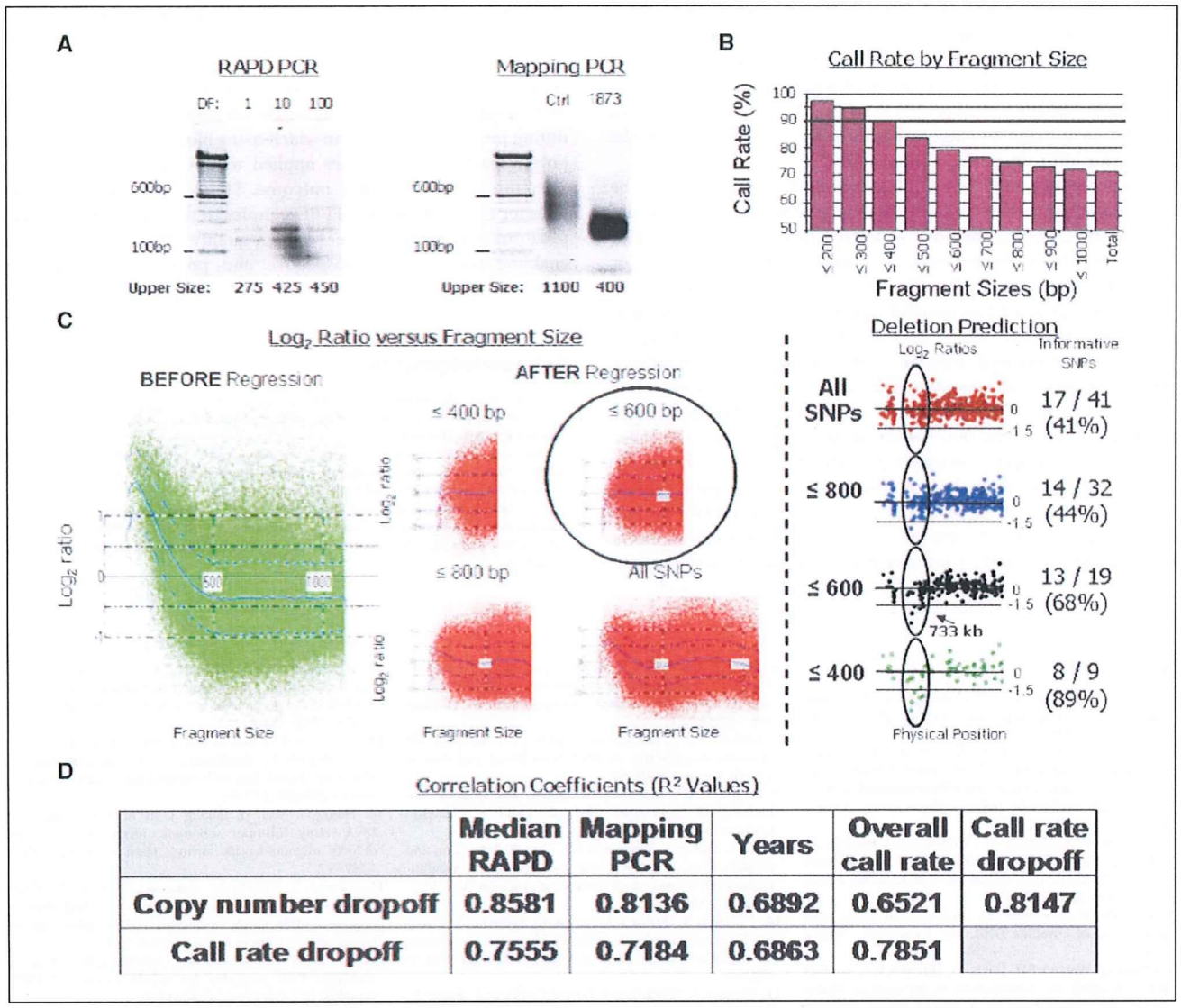

	Median RAPD	Mapping PCR	Years	Overall call rate	Call rate dropoff
Copy number dropoff	0.8581	0.8136	0.6892	0.6521	0.8147
Call rate dropoff	0.7555	0.7184	0.6863	0.7851	

Figure 4. Prediction of FFPE sample performance. *A*, display of RAPD-PCR and Mapping assay PCR for a single breast tumor sample (1873). Maximum size amplicons from RAPD-PCR varied from 275 to 450 bp, with dilution factors (*DF*) of 1, 10, and 100. Although high-quality DNA had a maximum upper fragment size of ~1,100 after PCR during the Mapping assay, this sample was well amplified only up to ~400 bp. *B*, call rate by fragment size was monitored for the same sample, using a stringent confidence value threshold of 0.26. Call rates dropped <90% when excluding SNPs on fragment sizes >400 bp. *C*, copy number versus fragment size plots in CNAG_v2.0 show a strong influence by fragment size on copy number predictions before correction (*left*). Regression corrects this bias somewhat, and more and more stringent filters further correct this bias (*middle*). With a filter excluding SNPs on fragment sizes >600 bp, the mean copy number (*blue line*) is consistent regardless of fragment size, indicating that this sample requires a copy number filter at 600 bp. Log 2 ratios produced using various fragment size filters are displayed for a region containing a 733-kb deletion on part of chromosome X. Under "Informative SNPs," the number of SNPs predicting a deletion with a log 2 ratio below −0.3 (considered to be "informative") are listed to the left of the number of total SNPs within the deletion region that were retained during the fragment size filter. Below these values is the percentage of SNPs included in the analysis that were informative of the deletion. *D*, R^2 regression values when the fragment size at which call rates drop <90% or the maximum fragment size that can be included in copy number analyses are compared with median maximum RAPD-PCR amplicon size, maximum Mapping PCR amplicon size, years of storage, or overall call rate ($P \leq 0.26$) are displayed. PCR tests better predicted copy number performance than years of storage or overall call rate, and they were better predictors of genotype performance than years of storage was.

both extent of DNA degradation and modification as well as the amount of inhibitors remaining in the sample. Use of a suitable DNA extraction protocol, such as the DNeasy Tissue kit, is important for obtaining DNA amenable to the assay, but other factors, such as years of storage and fixation process, will be harder to control. This underscores the necessity for a pre-WGSA quality control step that includes PCR of larger fragment sizes, such as RAPD-PCR or multiplex PCR (16). This study attempts to outline guidelines for qualifying FFPE DNA samples and analyzing qualified samples, but not all FFPE blocks will yield DNA suitable for the Mapping arrays.

FFPE DNA that is applied to the arrays may still vary in quality and therefore require more or less stringent fragment size filters. Despite reduction in coverage to accommodate loss of larger fragments, high resolution for genotype, LOH, and copy number assessment can still be maintained (Table 2; Supplementary Fig. S1). This is true because of the large number of SNPs on small fragments and because fragment size seems to be the only limiting

factor. For example, with exclusion of SNPs on amplicons >700 bp, as was required for the first set of five FFPE samples, 308,788 SNPs were retained for analysis, providing a median and mean inter-SNP distance of 4.3 or 9.5 kb, respectively. Although the 10K array is also suitable for analysis of degraded DNA (3), the large SNP coverage and the small fragment emphasis of the Mapping 500K arrays make it ideal for FFPE sample analysis.

The percentage of FFPE samples archived in banks that could be applied to the arrays with limited loss in genomic resolution would be influenced by the methods of fixation and extraction used at various institutes. Importantly, all samples stored for 6 years or fewer provided copy number data for a minimum of 234K SNPs in this study. Some of the samples applied to the arrays required extremely stringent filters against fragment size, resulting in significantly decreased resolution of genomic data. Potentially, researchers may choose only to analyze DNA samples of such low quality when the FFPE sample is considered to be particularly precious. Importantly, RAPD-PCR results predicted that these samples would display decreased performance on the array and a PCR screen could be applied to avoid application of poorly doing samples. With the advent of more standardized protocols for sample processing in the future and with advances in DNA extraction, a higher proportion of FFPE samples may be applicable to the arrays.

Despite the large banks of FFPE samples available for retrospective studies that include follow-up analysis of patient outcome, most of these studies currently focus on frozen samples because of the limited options available for paraffin samples. Additionally, FFPE processing holds advantages for tissue storage during prospective studies, in which many biopsies are collected but only a fraction of them are applied to downstream assays with selection based on clinical outcome. These results outline guidelines for the application of FFPE samples to the same genome-wide platform already available to high-quality DNA samples, thus enabling widespread retrospective and prospective analysis of tumor samples in their most common form of storage.

Acknowledgments

Received 10/2/2006; revised 12/19/2006; accepted 1/8/2007.

Grant support: National Breast Cancer Foundation postgraduate research scholarship (E.R. Thompson).

The costs of publication of this article were defrayed in part by the payment of page charges. This article must therefore be hereby marked *advertisement* in accordance with 18 U.S.C. Section 1734 solely to indicate this fact.

We would like to thank Giulia Kennedy, Manqiu Cao, Yaron Turpaz, and Guoliang Xing for technical input and discussions, Michael Shapero for his helpful suggestions and critical reading of the manuscript, and Dr. Alex Dobrovic for his help with DNA extraction.

References

1. Wang Y, Moorhead M, Karlin-Neumann G, et al. Allele quantification using molecular inversion probes (MIP). Nucleic Acids Res 2005;33:e183.
2. Lips EH, Dierssen JW, van Eijk R, et al. Reliable high-throughput genotyping and loss-of-heterozygosity detection in formalin-fixed, paraffin-embedded tumors using single nucleotide polymorphism arrays. Cancer Res 2005;65:10188–91.
3. Thompson ER, Herbert SC, Forrest SM, Campbell IG. Whole genome SNP arrays using DNA derived from formalin-fixed, paraffin-embedded ovarian tumor tissue. Hum Mutat 2005;26:384–9.
4. Kennedy GC, Matsuzaki H, Dong S, et al. Large-scale genotyping of complex DNA. Nat Biotechnol 2003;21: 1233–7.
5. Bryan EJ, Watson RH, Davis M, Hitchcock A, Foulkes WD, Campbell IG. Localization of an ovarian cancer tumor suppressor gene to a 0.5-cM region between D22S284 and CYP2D, on chromosome 22q. Cancer Res 1996;56:719–21.
6. Jiang X, Hitchcock A, Bryan EJ, et al. Microsatellite analysis of endometriosis reveals loss of heterozygosity at candidate ovarian tumor suppressor gene loci. Cancer Res 1996;56:3534–9.
7. Mullenbach R, Lagoda PJL, Welter C. An efficient salt chloroform extraction of DNA from blood and tissues. Trends Genet 1989;5:391.
8. Bancroft JD, Stevens A. Theory and practice of histological techniques. 3rd ed. London: Churchill Livingstone; 1991. p. 48–57.
9. Wu L, Patten N, Yamashiro CT, Chui B. Extraction and amplification of DNA from formalin-fixed, paraffin-embedded tissues. Appl Immunohistochem Mol Morphol 2002;10:269–74.
10. Williams JG, Kubelik AR, Livak KJ, Rafalski JA, Tingey SV. DNA polymorphisms amplified by arbitrary primers are useful as genetic markers. Nucleic Acids Res 1990;18: 6531–5.
11. Siwoski A, Ishkanian A, Garnis C, Zhang L, Rosin M, Lam WL. An efficient method for the assessment of DNA quality of archival microdissected specimens. Mod Pathol 2002;15:889–92.
12. Di X, Matsuzaki H, Webster TA, et al. Dynamic model based algorithms for screening and genotyping over 100 K SNPs on oligonucleotide microarrays. Bioinformatics 2005;21:1958–63.
13. Lin M, Wei LJ, Sellers WR, Lieberfarb M, Wong WH, Li C. dChipSNP: significance curve and clustering of SNP-array-based loss-of-heterozygosity data. Bioinformatics 2004;20:1233–40.
14. Huang J, Wei W, Zhang J, et al. Whole genome DNA copy number changes identified by high density oligonucleotide arrays. Hum Genomics 2004; 1:287–99.
15. Nannya Y, Sanada M, Nakazaki K, et al. A robust algorithm for copy number detection using high-density oligonucleotide single nucleotide polymorphism genotyping arrays. Cancer Res 2005;65:6071–9.
16. van Beers EH, Joosse SA, Ligtenberg MJ, et al. A multiplex PCR predictor for aCGH success of FFPE samples. Br J Cancer 2006;94:333–7.
17. Liu WM, Di X, Yang G, et al. Algorithms for large-scale genotyping microarrays. Bioinformatics 2003;19: 2397–403.

Available online at www.sciencedirect.com
ScienceDirect
Biochemical and Biophysical Research Communications 354 (2007) 892–898
BBRC
www.elsevier.com/locate/ybbrc

Functional characterization of a new p53 mutant generated by homozygous deletion in a neuroblastoma cell line

Yohko Nakamura [1], Toshinori Ozaki [1], Hidetaka Niizuma, Miki Ohira, Takehiko Kamijo, Akira Nakagawara *

Division of Biochemistry, Chiba Cancer Center Research Institute, Chiba 260-8717, Japan

Received 11 January 2007
Available online 22 January 2007

Abstract

p53 is a key modulator of a variety of cellular stresses. In human neuroblastomas, p53 is rarely mutated and aberrantly expressed in cytoplasm. In this study, we have identified a novel p53 mutant lacking its COOH-terminal region in neuroblastoma SK-N-AS cells. p53 accumulated in response to cisplatin (CDDP) and thereby promoting apoptosis in neuroblastoma SH-SY5Y cells bearing wild-type *p53*, whereas SK-N-AS cells did not undergo apoptosis. We found another p53 (p53ΔC) lacking a part of oligomerization domain and nuclear localization signals in SK-N-AS cells. p53ΔC was expressed largely in cytoplasm and lost the transactivation function. Furthermore, a 3′-part of the *p53* locus was homozygously deleted in SK-N-AS cells. Thus, our present findings suggest that p53 plays an important role in the DNA-damage response in certain neuroblastoma cells and it seems to be important to search for *p53* mutations outside DNA-binding domain.

Keywords: Apoptosis; Cisplatin; Homozygous deletion; Neuroblastoma; p53

p53 plays a pivotal role in the regulation of cell cycle arrest and apoptosis. *p53* is one of the most frequently mutated genes in human tumors [1,2] and *p53*-deficient mice developed spontaneous tumors [3]. Upon a variety of cellular stresses, p53 accumulates in nucleus through post-translational modifications including phosphorylation and acetylation and thereby exerting its function [4]. Pro-apoptotic function of p53 is closely linked to its DNA-binding activity. p53 acts as a transcription factor to transactivate a variety of its target genes. Indeed, 95% of *p53* mutations in human tumors occur within its DNA-binding region and these mutations inactivate pro-apoptotic function of p53 [4].

Alternatively, p53 is inhibited by various mechanisms. MDM2 acts as an E3 ubiquitin ligase for p53 and promotes its proteolytic degradation through ubiquitin–proteasome pathway [5,6]. Subcellular distribution of p53 also plays a key role in the regulation of p53 [4]. p53 contains three nuclear localization signals (NLS I, II, and III) in its COOH-terminal region [7,8]. In contrast to other human tumors, *p53* is rarely mutated in neuroblastomas [9]. Neuroblastoma cells showed a cytoplasmic localization of wild-type p53 and exhibited an impaired p53-mediated cell cycle arrest in response to DNA damage, suggesting that there exists a mutation-independent mechanism of p53 inactivation [10–12]. Intriguingly, Nikolaev et al. demonstrated that Parkin-like ubiquitin ligase termed Parc serves as an anchor protein that tethers p53 in cytoplasm and thereby regulating subcellular localization and function of p53 [13].

In this study, we have identified a novel p53 mutant (p53ΔC) homozygously deleted in neuroblastoma SK-N-AS cells and our current studies suggest that *p53* status plays an important role in the cell fate determination of certain neuroblastoma cells in response to DNA damage.

* Corresponding author. Fax: +81 43 265 4459.
E-mail address: akiranak@chiba-cc.jp (A. Nakagawara).
[1] These authors contributed equally to this work.

0006-291X/$ - see front matter © 2007 Elsevier Inc. All rights reserved.
doi:10.1016/j.bbrc.2007.01.057

Materials and methods

Cell culture and transfection. Neuroblastoma cells were grown in RPMI 1640 medium supplemented with 10% heat-inactivated fetal bovine serum (FBS, Invitrogen) and antibiotic mixture in a humidified atmosphere of 5% CO_2 in air at 37 °C. For transfection, cells were transfected with the indicated expression plasmids using LipofectAMINE 2000 according to the manufacturer's instructions (Invitrogen).

Construction of p53 mutant. cDNA encoding p53 mutant was amplified by PCR using cDNA from SK-N-AS cells. Forward and reverse primers were 5′-**AATATT**TCACCCTTCAGGTACTAAG-3′ (forward) and 5′-**CTCGAG**TCACTGCCCCCTGATGGC-3′ (reverse). *Ssp*I and *Xho*I sites shown in boldface type were introduced into forward and reverse primers, respectively. PCR products were gel-purified and subcloned into pGEM-T plasmid (Promega). Constructs were confirmed by sequencing and then digested with *Ssp*I and *Xho*I. The digested fragment was again gel-purified and then ligated with the *Ssp*I and *Bam*HI fragment of FLAG-p53 to give pcDNA3-FLAG-p53CΔ.

RNA preparation and RT-PCR analysis. Total RNA was prepared using RNeasy Mini kit (Qiagen) following the manufacturer's protocol. cDNA was synthesized using SuperScript II with random primers (Invitrogen) and amplified by PCR using primers as described: *p53*: forward, 5′-CTGCCCTCAACAAGATGTTTTG-3′, and reverse, 5′-CTATCTGAGCAGCGCTCATGG-3′; $p21^{WAF1}$: forward, 5′-ATGAAATTCACCCCCTTTCC-3′, and reverse, 5′-CCCTAGGCTGTGCTCACTTC-3′; *Bax*: forward, 5′-TTTGCTTCAGGGTTTCATCC-3′, and reverse, 5′-CAGTTGAAGTTGCCGTCAGA-3′; *p53AIP1*: forward, 5′-CCAAGTTCTCTGCTTTC-3′ and reverse, 5′-AGCTGAGCTCAAATGCTGAC-3′; *PUMA*: forward, 5′-TATGGATCCCGCACCATGGACTACAAGGACGACGATGACAAGGCCCGCGCACGCCAG-3′ and reverse, 5′-TATGGATCCCTACATGGTGCAGAGAAAGTCCCCC-3′; and *GAPDH*: forward, 5′-ACCTGACCTGCCGTCTAGAA-3′, and reverse, 5′-TCCACCACCCTGTTGCTGTA-3′.

Southern blotting. Genomic DNA was digested with *Pst*I, separated by 1% agarose gel electrophoresis, and transferred onto nylon membranes. Hybridization was performed at 65 °C in a solution containing 1 M NaCl, 1% *N*-lauroyl sarcosine, 7.5% dextran sulfate, 100 μg of heat-denatured salmon sperm DNA/ml, and radio-labeled DNA. After hybridization, membranes were washed twice with 2× SSC/0.1% *N*-lauroyl sarcosine at 50 °C and exposed to an X-ray film at −70 °C.

Immunoblotting. Cells were lysed in lysis buffer containing 25 mM Tris–HCl, pH 8.0, 137 mM NaCl, 2.7 mM KCl, 1% Triton X-100, and protease inhibitor mixture (Sigma). Lysates were separated by SDS–PAGE and transferred onto Immobilon-P membranes (Millipore). Membranes were probed with anti-p53 (DO-1, Calbiochem), anti-p53 (PAb122, BD Pharmingen), anti-phosphorylated p53 at Ser-15 (Cell Signaling) or with anti-actin (20–33, Sigma) followed by incubation with HRP-conjugated goat anti-mouse or anti-rabbit IgG secondary antibody (Cell Signaling). Immunoreactive bands were detected using chemiluminescence (ECL, Amersham Biosciences).

Subcellular fractionation. Cells were lysed in lysis buffer containing 10 mM Tris–HCl, pH 7.5, 1 mM EDTA, 0.5% NP-40, and protease inhibitor mixture (Sigma). Lysates were centrifuged to separate soluble (cytosolic) from insoluble (nuclear) fractions. The nuclear and cytosolic fractions were subjected to immunoblotting using anti-p53, anti-Lamin B (Ab-1, Oncogene Research products) or with anti-tubulin-α (Ab-2, NeoMarkers).

Array-based comparative genomic hybridization (CGH) analysis. Whole genome arrays of 2464 bacterial artificial chromosome (BAC) clones were hybridized simultaneously with 500 ng of target DNA (SK-N-AS, RTBM1, and SH-SY5Y) and reference DNA (normal female genomic DNA). Target DNAs were labeled with Cy3-dCTP and reference DNAs with Cy5-dCTP by random priming. Hybridization, scanning, and data processing were conducted as described previously [14,15].

Cell survival assays. Cells were plated at a density of 5000 cells/well in 96-well tissue culture plates. After attachment overnight, medium was replaced and treated with CDDP for 24 h. Cell viability was measured by MTT assay.

Flow cytometry. Floating and adherent cells were pooled and fixed in ice-cold 70% ethanol for 4 h at −20 °C. Cells were then stained with 10 mg/ml of PI (Sigma) in the presence of 250 mg/ml of RNase A at 37 °C for 30 min in the dark. Number of cells with sub-G1 DNA content was measured by flow cytometry (FACScan, Becton–Dickinson).

TUNEL assay. Apoptotic cells were identified using an *in situ* cell detection, peroxidase kit (Roche Applied Science). Briefly, cells were fixed in 4% paraformaldehyde and permeabilized with 0.1% Triton X-100. The labeling reaction was performed using TMR red-labeled dUTP together with other nucleotides by terminal deoxynucleotidyl transferase for 1 h in the dark at 37 °C. Then, cells were mounted and the incorporated TMR red-labeled dUTP was analyzed using a Fluoview laser scanning confocal microscope (Olympus).

Luciferase reporter assay. H1299 cells were co-transfected with pcDNA3, FLAG-p53 or FLAG-p53ΔC expression plasmid, p53-responsive luciferase reporter ($p21^{WAF1}$, *MDM2* or *Bax*), and pRL-TK *Renilla* luciferase cDNA. Forty-eight hours after transfection, firefly and *Renilla* luciferase activities were measured with dual-luciferase reporter assay system according to the manufacturer's instructions (Promega).

Colony formation assay. Forty-eight hours after transfection, SK-N-AS cells were transferred to fresh medium containing G418 (400 μg/ml). After 16 days of selection, drug-resistant colonies were fixed in methanol and stained with Giemsa's solution.

Results

DNA-damage response in human neuroblastoma cells

To determine the effects of genotoxic agents on neuroblastomas, human neuroblastoma SH-SY5Y and SK-N-AS cells were exposed to cisplatin (CDDP) and their viabilities were examined by MTT assays. As shown in Fig. 1A, their viabilities were significantly decreased in response to CDDP. To address whether CDDP could induce apoptosis, we performed TUNEL assay. As shown in Fig. 1B, we observed a higher number of TUNEL-positive SH-SY5Y cells exposed to CDDP, whereas CDDP had undetectable effects on SK-N-AS cells. We further determined apoptotic cells as sub-G1 population by flow cytometry. As seen in Fig. 1C, a significant increase in number of SH-SY5Y cells with sub-G1 DNA content was observed after CDDP treatment, whereas CDDP treatment of SK-N-AS cells resulted in an increase in S-phase cells but not in G2/M-phase cells. Consistent with these results, *thymidine kinase* (S-phase marker) [16] was increased in CDDP-treated SK-N-AS cells, whereas *Plk1* (M-phase marker) [17] remained unchanged regardless of CDDP treatment (data not shown).

We then examined whether p53-dependent apoptotic pathway could be activated in response to CDDP. As shown in Fig. 1D, p53 was phosphorylated at Ser-15 in SH-SY5Y cells exposed to CDDP. *p53* remained unchanged regardless of CDDP treatment, whereas p53 target genes including $p21^{WAF1}$, *Bax*, and *PUMA* were transactivated in response to CDDP. In contrast, CDDP-mediated phosphorylation of p53 at Ser-15 was undetectable in SK-N-AS cells. $p21^{WAF1}$ was induced in response to CDDP, however, CDDP-mediated up-regulation of pro-apoptotic *Bax* and *PUMA* was undetectable, suggesting that p53 pro-apoptotic function might be lost in SK-N-AS cells.

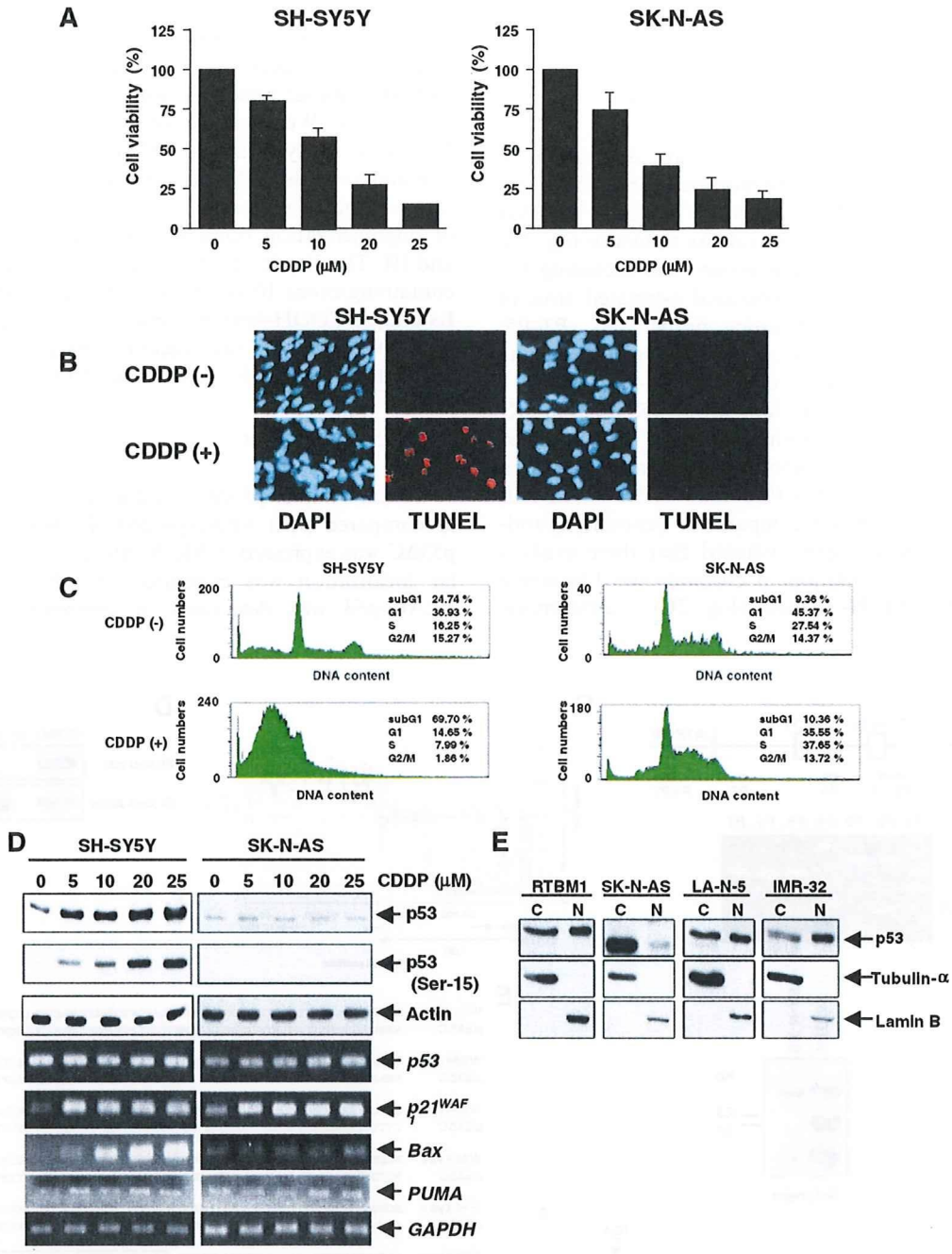

Fig. 1. Differential effects of CDDP on neuroblastoma cells. (A) Cell survival assays. Twenty-four hours after CDDP treatment, cell viability was analyzed by MTT assays. (B) TUNEL staining. Twenty-four hours after CDDP treatment (20 μM), apoptotic cells were detected by TUNEL staining. Cell nuclei were stained with DAPI. (C) FACS analysis. SH-SY5Y and SK-N-AS cells were treated as in (B). Twenty-four hours after CDDP treatment, cell cycle distributions were analyzed by FACS. Shown are the representatives of three independent experiments. (D) CDDP-induced accumulation of p53 in neuroblastoma cells. Twenty-four hours after CDDP treatment, lysates and total RNA were subjected to immunoblotting (upper panels) and RT-PCR (lower panels), respectively. For protein loading control, actin levels were checked by immunoblotting. For RT-PCR, *GAPDH* was used as a loading control. (E) Subcellular localization of p53. The indicated neuroblastoma cells were fractionated into cytoplasmic (C) and nuclear (N) fractions and subcellular distribution of p53 was analyzed by immunoblotting. Tubulin-α and Lamin B were used as cytoplasmic and nuclear markers, respectively.

To investigate molecular mechanism(s) behind p53 dysfunction in SK-N-AS cells, we examined subcellular localization of p53 in various neuroblastoma cells. As shown in Fig. 1E, p53 was detected in cytoplasm and nucleus of RTBM1, LA-N-5, and IMR-32 cells bearing wild-type *p53* (data not shown). Of note, p53 was abundantly expressed in cytoplasm of SK-N-AS cells and its molecular mass was smaller than those of other

cells, indicating that it might be due to certain structural aberrations.

Structural aberration of p53 in SK-N-AS cells

To address whether p53 could have any aberrations in SK-N-AS cells, we amplified the indicated genomic regions of *p53* using genomic DNA from SK-N-AS cells. RTBM1 cells were used as a positive control. As shown in Fig. 2A, PCR-based amplification using primer sets including P1, P2, P6, and P7 successfully generated estimated sizes of PCR products, whereas remaining primer sets (P3–P5) did not, suggesting that the genomic region containing exons 10 and 11 of *p53* might be lost in SK-N-AS cells.

To confirm genomic aberrations within *p53* locus in SK-N-AS cells, we performed Southern analysis. Radio-labeled *p53* cDNA probe failed to detect *Pst*I fragment (2.0 kb in length) which contains exons 10 and 11 in SK-N-AS cells (Fig. 2B). Our array-based comparative genomic hybridization (CGH) analysis demonstrated that there exists a large range of allelic deletion of chromosome 17p where *p53* is located in SK-N-AS cells (Fig. 2C). Furthermore, anti-p53 antibody which recognizes p53 extreme COOH-terminal portion could not detect p53 in SK-N-AS cells (Fig. 2D). Collectively, our results suggest that p53 COOH-terminal region is homozygously deleted in SK-N-AS cells. We then cloned *p53* cDNA. As shown in Fig. 2E, a newly identified p53 (p53ΔC) was composed of 369 amino acids including unique COOH-terminal structure (estimated molecular mass of 49 kDa), lacked a part of oligomerization domain, and completely lost NLS II and III. The 3′-side of intron 9 and the downstream region containing exons 10 and 11 were deleted in SK-N-AS cells. Its unique COOH-terminal amino acids were derived from intron 9, suggesting that accurate splicing event might be abrogated and thereby generating p53ΔC.

Dysfunction of p53ΔC

To ask whether p53ΔC could have functional differences as compared with wild-type p53, FLAG-p53 or FLAG-p53ΔC was expressed in SK-N-AS cells and their subcellular localization was examined. As shown in Fig. 3A, FLAG-p53 was detectable in cytoplasm and nucleus,

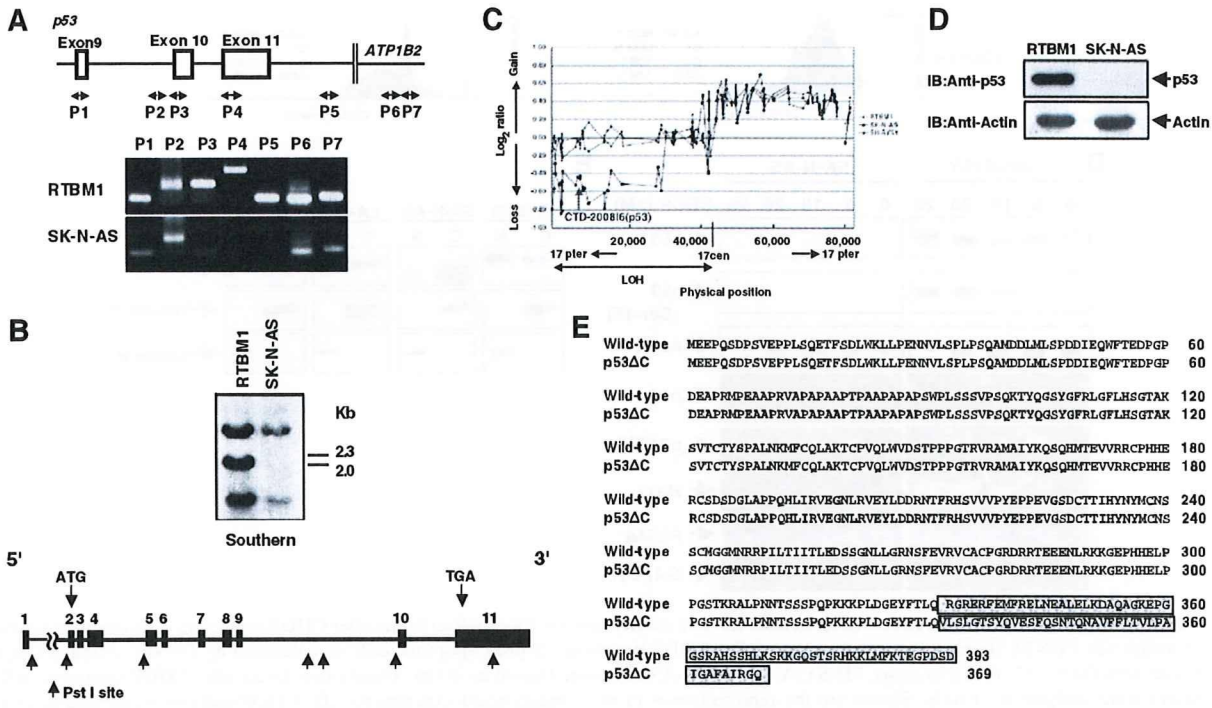

Fig. 2. p53 COOH-terminal region is deleted in SK-N-AS cells. (A) Genomic structure of human *p53* locus and positions of PCR primers (P1–P7) are shown. *ATP1B2* encodes ATPase, Na^+/K^+ transporting β2 (upper panel). Genomic DNA from RTBM1 and SK-N-AS cells was subjected to PCR using the indicated primers (lower panels). (B) Southern blot analysis. Genomic DNA was digested with *Pst*I, separated by 1% agarose gel, transferred onto nylon membrane, and probed with the radio-labeled *p53* cDNA. Schematic diagram of human *p53* and positions of *Pst*I sites are also shown. (C) Array-based comparative genomic hybridization (CGH) analysis. Hybridization was performed as described under Materials and methods. Arrays were scanned and images processed using custom software. We normalized relative ratios of tumor and normal signals by setting the value of the median relative ratio equal to 1. The data were then transformed into log 2 space and plotted as a histogram to determine cutoffs for scoring loss or gain. Three Gaussian distribution curves were fitted to the histogram, and values >3 SD from the central Gaussian were scored as losses or gains for that tumor. (D) Immunoblotting. Lysates from RTBM1 and SK-N-AS were processed for immunoblotting with the specific antibody against p53 extreme COOH-terminal portion. (E) Amino acid sequence alignment of wild-type p53 and p53ΔC. The different amino acid residues between them are boxed.

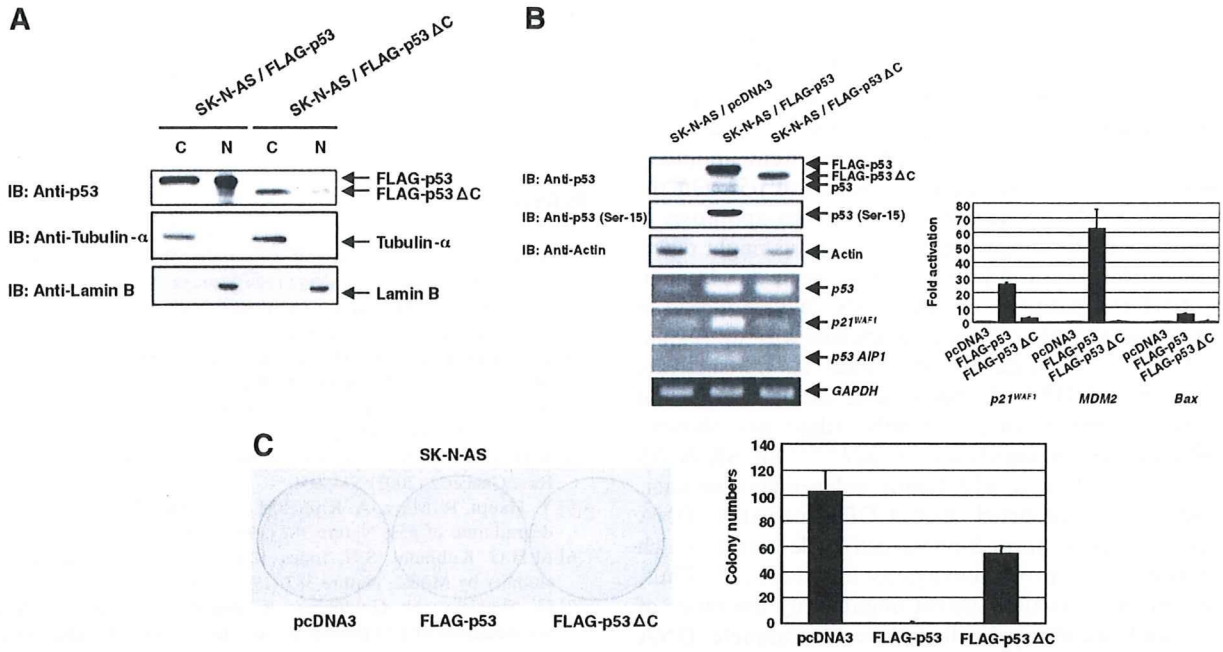

Fig. 3. Loss of function of p53ΔC. (A) Subcellular localization of exogenously expressed wild-type p53 and p53ΔC. SK-N-AS cells were transfected with the indicated expression plasmids. Forty-eight hours after transfection, cells were fractionated into cytoplasmic (C) and nuclear (N) fractions followed by immunoblotting with anti-p53 antibody. (B) Possible effects of COOH-terminal deletion of p53 on its transcriptional activity. SK-N-AS cells were transfected with the indicated expression plasmids. Forty-eight hours after transfection, lysates and total RNA were subjected to immunoblotting and RT-PCR, respectively (left panel). (Right panel) Luciferase reporter assays. *p53*-deficient H1299 cells were co-transfected with pcDNA3, FLAG-p53 or FLAG-p53ΔC expression plasmid, p53-responsive luciferase reporter ($p21^{WAF1}$, *MDM2* or *Bax*) and *Renilla* luciferase cDNA. Forty-eight hours after transfection, luciferase activities were measured. (C) Colony formation assay. Forty-eight hours after transfection, SK-N-AS cells were transferred to fresh medium containing G418 (400 μg/ml). Sixteen days after selection with G418, drug-resistant colonies were stained with Giemsa's solution (left panel) and the number of colonies was scored (right panel).

whereas FLAG-p53ΔC was largely expressed in cytoplasm. Next, we examined transcriptional potential of p53ΔC in SK-N-AS cells. As seen in left panel of Fig. 3B, FLAG-p53 but not FLAG-p53ΔC was phosphorylated at Ser-15. Consistent with these results, FLAG-p53 transactivated $p21^{WAF1}$ and *p53AIP1*. In contrast, FLAG-p53ΔC failed to transactivate $p21^{WAF1}$ and *p53AIP1*. Similar results were also obtained by luciferase reporter assays (Fig. 3B, right panel). To examine effects of COOH-terminal deletion on pro-apoptotic activity of p53, we performed colony formation assays. SK-N-AS cells were transfected with empty plasmid, FLAG-p53 or FLAG-p53ΔC expression plasmid and maintained in medium containing G418 for 16 days. As shown in Fig. 3C, number of drug-resistant colonies was significantly reduced in cells expressing FLAG-p53. Intriguingly, enforced expression of FLAG-p53ΔC resulted in a decrease in number of drug-resistant colonies but to a lesser degree as compared with that in cells expressing FLAG-p53. These observations suggest that COOH-terminal deletion reduces transcriptional and pro-apoptotic activities of p53.

Discussion

In this study, we have identified p53ΔC in SK-N-AS cells. Consistent with the recent report [13], p53 was predominantly expressed in cytoplasm of SK-N-AS cells. According to their results, Parc inhibited p53 nuclear translocation through the direct interaction with its COOH-terminal region. Since p53 contains three NLSs in its COOH-terminal region, Parc might inhibit its nuclear access by masking its NLSs [13]. In accordance with these findings, p53 COOH-terminal peptide inhibited its cytoplasmic retention [12]. Based on our immunoprecipitation experiments, wild-type p53 but not p53ΔC was co-immunoprecipitated with the endogenous Parc in SK-N-AS cells (data not shown), suggesting that cytoplasmic retention of p53ΔC is regulated in a Parc-independent manner. p53ΔC lacks NLS II and III but retains NLS I. Although Kim et al. described that importin-α interacts with NLS I of p53 and mediates its nuclear import [18], NLS II and/or III might play a major role in nuclear import of p53 in SK-N-AS cells.

p53 phosphorylation is significantly associated with its pro-apoptotic function [4]. Exogenously expressed wild-type p53 but not p53ΔC was phosphorylated at Ser-15 in SK-N-AS cells without DNA damage and transactivated $p21^{WAF1}$ and *p53AIP1*. Rodicker and Putzer described that exogenously expressed p53 is phosphorylated at Ser-15 without DNA damage [19]. Although it is unknown why exogenously expressed p53 but not p53ΔC is phosphorylated at Ser15 without DNA damage, it might be at least

in part due to its cytoplasmic retention. Colony formation assays demonstrated that wild-type p53 markedly reduces number of drug-resistant colonies in SK-N-AS cells, suggesting that there might not exist functional disruptions of downstream mediators of p53 in SK-N-AS cells. In response to CDDP, SH-SY5Y cells underwent apoptosis in association with a significant induction of p53. On the other hand, SK-N-AS cells did not undergo apoptosis in response to CDDP, suggesting that *p53* status might determine neuroblastoma cell fate to survive or to die. Intriguingly, CDDP treatment of SK-N-AS cells induced an accumulation of S-phase cells accompanied with up-regulation of $p21^{WAF1}$. Since p53ΔC failed to transactivate $p21^{WAF1}$ and CDDP had undetectable effects on *p73* and *p63* (other members of *p53* family) (data not shown), CDDP-mediated up-regulation of $p21^{WAF1}$ in SK-N-AS cells is regulated in a p53 family-independent manner. Knudsen et al. reported that CDDP-mediated DNA damage induces an intra-S-phase cell cycle arrest, which is correlated with a protection against apoptosis [20]. Thus, the genome maintenance system might delay the onset of mitosis, and thereby providing time to complete DNA repair and/or DNA replication before cell division in SK-N-AS cells. Further efforts should be necessary to address this issue.

Majority of *p53* mutations is detected within its DNA-binding region [21]. SK-N-AS cells have been believed to express wild-type p53 [22]. Much of information regarding *p53* mutations was derived from sequence analysis of exons 5–8 which encode its DNA-binding domain [4]. Indeed, there exist missense mutations in p53 oligomerization domain [23]. According to their results, Leu to Pro substitution at 344 inhibited the oligomerization of p53 and abolished its DNA-binding activity. Since p53ΔC lacks a part of oligomerization domain including Leu-344, p53ΔC might exist as a monomeric latent form. Recently, Bourdon et al. described that human *p53* is expressed as multiple isoforms including p53β and p53γ [24]. Based on amino acid sequence comparison, p53ΔC was distinct from p53β and p53γ (data not shown). During the preparation of our manuscript, Goldschneider et al. reported that SK-N-AS cells express p53β [25]. This discrepancy might be attributed to co-expression of p53β and p53ΔC in SK-N-AS cells and/or due to the acquired heterogeneity of SK-N-AS cells during culture. Additionally, murine *p53* expresses an alternative splicing isoform termed ASp53 with different COOH-terminus from that of wild-type p53 [26]. ASp53 displays an enhanced transcriptional activity as compared with wild-type p53, indicating that p53ΔC is distinct from human counterpart of ASp53.

Acknowledgments

This work was supported in part by a Grant-in-Aid from the Ministry of Health, Labor and Welfare for Third Term Comprehensive Control Research for Cancer, a Grant-in-Aid for Scientific Research on Priority Areas from the Ministry of Education, Culture, Sports, Science and Technology, Japan, a Grant-in-Aid for Scientific Research from Japan Society for the Promotion of Science, and a Grant from Uehara Memorial Foundation.

References

[1] M. Hollstein, D. Sidransky, B. Vogelstein, H. Harris, p53 mutations in human cancers, Science 253 (1991) 49–53.
[2] A.J. Levine, J. Momand, C.A. Finlay, The p53 tumour suppressor gene, Nature 351 (1991) 453–456.
[3] L.A. Donehower, M. Harvey, B.L. Slagle, M.J. McArthur, C.A. Montgomery Jr., J.S. Butel, A. Bradley, Mice deficient for p53 are developmentally normal but susceptible to spontaneous tumours, Nature 356 (1992) 215–221.
[4] K.H. Vousden, X. Lu, Live or let die: the cells response to p53, Nat. Rev. Cancer 2 (2002) 594–604.
[5] Y. Haupt, R. Maya, A. Kazaz, M. Oren, Mdm2 promotes the rapid degradation of p53, Nature 387 (1997) 296–299.
[6] M.H.G. Kubbutat, S.N. Jones, K.H. Vousden, Regulation of p53 stability by Mdm2, Nature 387 (1997) 299–303.
[7] G. Shaulsky, N. Goldfinger, A. Ben-Ze'ev, V. Rotter, Nuclear accumulation of p53 protein is mediated by several nuclear localization signals and plays a role in tumorigenesis, Mol. Cell. Biol. 10 (1990) 6565–6577.
[8] S.H. Liang, D. Hong, M.F. Clarke, Cooperation of a single lysine mutation and a C-terminal domain in the cytoplasmic sequestration of the p53 protein, J. Biol. Chem. 273 (1998) 19817–19821.
[9] K. Vogan, M. Bernstein, J.M. Leclerc, L. Brisson, J. Brossard, G.M. Brodeur, J. Pelletier, P. Gros, Absence of p53 gene mutations in primary neuroblastomas, Cancer Res. 53 (1993) 5269–5273.
[10] U.M. Moll, M. LaQuaglia, J. Benard, G. Riou, Wild-type p53 protein undergoes cytoplasmic sequestration in undifferentiated neuroblastomas but not in differentiated tumors, Proc. Natl. Acad. Sci. USA 92 (1995) 4407–4411.
[11] U.M. Moll, A.G. Ostermeyer, R. Haladay, B. Winkfield, M. Frazier, G. Zambetti, Cytoplasmic sequestration of wild-type p53 protein impairs the G1 checkpoint after DNA damage, Mol. Cell. Biol. 16 (1996) 1126–1137.
[12] A.G. Ostermeyer, E. Runko, B. Winkfield, B. Ahn, U.M. Moll, Cytoplasmically sequestrated wild-type p53 protein in neuroblastoma is relocated to the nucleus by a C-terminal peptide, Proc. Natl. Acad. Sci. USA 93 (1996) 15190–15194.
[13] A.Y. Nikolaev, M. Li, N. Puskas, J. Qin, W. Gu, Parc: A cytoplasmic anchor for p53, Cell 112 (2003) 29–40.
[14] A.M. Snijders, N. Nowak, R. Segraves, S. Blackwood, N. Brown, J. Conroy, G. Hamilton, A.K. Hindle, B. Huey, K. Kimura, S. Law, K. Myambo, J. Palmer, B. Yistra, J.P. Yue, J.W. Gray, A.N. Jain, D. Pinkel, D.G. Albertson, Assembly of microarrays for genome-wide measurement of DNA copy number, Nat. Genet. 29 (2001) 263–264.
[15] J.M. Nigro, A. Misra, L. Zhang, I. Smimov, H. Colman, C. Griffin, N. Ozburn, M. Chen, E. Pan, D. Koul, W.K. Yung, B.G. Feuerstein, K.D. Aldape, Integrated array-comparative genomic hybridization and expression array profiles identity clinically relevant molecular subtypes of glioblastoma, Cancer Res. 65 (2005) 1678–1686.
[16] D.L. Coppock, A.B. Pardee, Control of thymidine kinase mRNA during the cell cycle, Mol. Cell. Biol. 7 (1987) 2925–2932.
[17] R. Hamanaka, M.R. Smith, P.M. O'Connor, S. Maloid, K. Mihalic, J.L. Spivak, D.L. Longo, D.K. Ferris, Polo-like kinase is a cell cycle-regulated kinase activated during mitosis, J. Biol. Chem. 270 (1995) 21086–21091.
[18] I.S. Kim, D.H. Kim, S.M. Han, M.U. Chin, H.J. Nam, H.P. Cho, S.Y. Choi, B.J. Song, E.R. Kim, Y.S. Bae, Y.H. Moon, Truncated form of importin α identified in breast cancer cell inhibits nuclear import of p53, J. Biol. Chem. 275 (2000) 23139–23145.

[19] F. Rodicker, B.M. Putzer, p73 is effective in p53-null pancreatic cancer cells resistant to wild-type TP53 gene replacement, Cancer Res. 63 (2003) 2737–2741.
[20] K.E. Knudsen, D. Booth, S. Naderi, Z. Sever-Chroneos, A.F. Fribourg, C. Hunton, J.R. Feramisco, J.Y.J. Wang, E.S. Knudsen, RB-dependent S-phase response to DNA damage, Mol. Cell. Biol. 20 (2000) 7751–7763.
[21] M. Hollstein, M. Hergenhahn, Q. Yang, H. Bartsch, Z.Q. Wang, P. Hainaut, New approaches to understanding p53 gene tumor mutation spectra, Mutat. Res. 431 (1999) 199–209.
[22] M. Kaghad, H. Bonnet, A. Yang, L. Creancier, J.C. Biscan, A. Valent, A. Minty, P. Chalon, J.M. Lelias, X. Dumont, P. Ferrara, F. McKeon, D. Caput, Monoallelically expressed gene related to p53 at 1p36, a region frequently deleted in neuroblastoma and other human cancers, Cell 90 (1997) 809–819.
[23] M.E. Lomax, D.M. Barnes, T.R. Hupp, S.M. Picksley, R.S. Camplejohn, Characterization of p53 oligomerization domain mutations isolated from Li-Fraumeni and Li-Fraumeni like family members, Oncogene 17 (1998) 643–649.
[24] J.C. Bourdon, K. Fernandes, F. Murray-Zmijewski, G. Liu, A. Diot, D.P. Xirodimas, M.K. Saville, D.L. Lane, p53 isoforms can regulates p53 transcriptional activity, Genes Dev. 19 (2005) 2122–2137.
[25] D. Goldschneider, E. Horvilleur, L.F. Plassa, M. Guillaud-Bataille, K. Million, E. Wittmer-Dupret, G. Danglot, H. de The, J. Benard, E. May, S. Douc-Rasy, Expression of C-terminal deleted p53 isoforms in neuroblastoma, Nucleic Acids Res. 34 (2006) 5603–5612.
[26] N. Arai, D. Nomura, K. Yokota, D. Wolf, E. Brill, O. Shohat, V. Rotter, Immunologically distinct p53 molecules generated by alternative splicing, Mol. Cell. Biol. 6 (1986) 3232–3239.

Leukemia (2007), 1–4

www.nature.com/leu

LETTER TO THE EDITOR

Clinical characteristics and outcomes in patients with t(8;21) acute myeloid leukemia in Japan

Leukemia advance online publication, 16 August 2007; doi:10.1038/sj.leu.2404905

In acute myeloid leukemia (AML), t(8;21)(q22;q22) translocation is one of the most common karyotype abnormalities, occurring in 7–8% of adult patients.[1] This change is closely associated with AML-M2 subtype in the French-American-British (FAB) classification, a type of AML with high complete remission (CR) rate (85–90%) and favorable survival rate.[1–3] Studies conducted in western countries have demonstrated that survival is prolonged when consolidation chemotherapies comprising high-dose cytarabine are administered.[2]

A research group from the Cancer and Leukemia Group B reported that clinical characteristics of t(8;21) AML could alter depending on ethnicity, suggesting that direct adoption of treatment strategies based on clinical studies conducted in western countries to Japanese patients may not be advisable.[4] A recent study from Japan focused mainly on the clinical impact of cytogenetics.[5] Information on clinical characteristics and optimal treatments, such as the clinical impact of high-dose cytarabine, thus remains unavailable for Japanese patients.

To establish optimal therapeutic strategies applicable to Japanese patients, clarification of clinical characteristics and outcomes in Japanese patients with t(8;21) AML is crucial. The present retrospective multicenter study was conducted to investigate the clinical characteristics of Japanese patients with t(8;21) AML.

From January 2000 to December 2005, a total of 147 Japanese adult patients (≥15-years-old), who were newly diagnosed with *de novo* AML (FAB: M2) according to FAB classifications, were consecutively enrolled in nine collaborating hospitals. We retrospectively reviewed the medical records of these patients. These 147 patients included 46 patients with t(8;21) AML and 101 AML(M2) patients without t(8;21).

Diagnosis of t(8;21) AML was established based on chromosomal analysis (G-banding, $n=45$) and/or detection of RUNX1(AML1)/MTG8(ETO) fusion gene by real-time reverse transcription-polymerase chain reaction ($n=16$). Overall survival was calculated from diagnosis to death from any causes and event-free survival was defined as the time from diagnosis to the following events: first relapse of AML; treatment-failure; or death from any cause except leukemia. High-, standard- and low-dose cytarabine were defined as ≥2 g/m^2/day, 100–200 mg/m^2/day and ≤40 mg/m^2/day, respectively. No patients received any other doses of cytarabine. Of the 46 patients with t(8;21), 4 were enrolled in the AML 202 study of the Japan Adult Leukemia Study Group.

Overall survival rate was calculated using the Kaplan-Meier product limit method. A log-rank test was applied to assess impact by the factor of interest when appropriate. Estimated survival was calculated as of January 31, 2007. Uni- and multivariate Cox proportional hazard models were applied to estimate the impact of potential prognostic factors. Factors associated with at least borderline significance ($P<0.10$) in univariate analyses were subjected to multivariate analysis using backward stepwise proportional-hazard modeling. Values of $P<0.05$ were considered statistically significant. Multivariate Cox proportional hazard models were used to determine the influence of age, sex and karyotype (with or without t(8;21)) on survival of all 147 patients. All analyses were conducted using STATA version 9.2 software (STATA, College Station, TX, USA).

Characteristics of AML patients with t(8;21) are shown in Table 1. Patients with t(8;21) (median age, 49.5 years; range, 18–86 years) were significantly younger than AML(M2) patients without t(8;21) (median age, 60 years; range 17–90 years; $P<0.001$). AML(M2) patients without t(8;21) included 57 men and 44 women. The median follow-up of surviving patients was 27.0 months (range, 0.2–82.6 months) after diagnosis.

Twelve patients with t(8;21) AML died during follow-up at a median of 10.6 months (range, 3.1–80.1 months) after diagnosis due to primary disease ($n=10$), pneumonia ($n=1$) or sudden cardiac death ($n=1$). Overall survival rates at 3 years after diagnosis in patients with t(8;21) was 70% (95% confidence interval (CI), 51–83%). This rate was significantly better than that in AML (M2) patients without t(8;21) (overall survival at 3 years, 0.43 (95%CI, 0.32–0.54); log-rank test, $P=0.005$; Figure 1a). Among patients <60-years-old, overall survival rates of patients with t(8;21) AML and patients with non-t(8;21) AML(M2) were 71% (95%CI, 47–86%) and 58% (95%CI, 41–72%), respectively (log-rank test, $P=0.28$; Figure 1b). Event-free survival rate at 3 years in patients with t(8;21) was 54% (95%CI, 37–69%). Overall survival rates in patients with t(8;21) according to karyotype are shown in Figure 1c. No significant difference in overall survival (Figure 1c) or event-free survivals were noted between karyotypic groups (log-rank test, $P=0.27$ and $P=0.51$, respectively). There was not any significant association between presence of extramedullary involvement and additional karyotype abnormality ($P=0.49$).

Of the 45 patients who received induction therapy, 36 and 5 patients achieved CR after first and second courses of chemotherapy, respectively (Table 1). CR rate was 91%.

Of the 40 patients who received induction therapy containing standard-dose cytarabine, 38 achieved CR. Among those, 21 patients received high-dose cytarabine-containing consolidation therapy. One of the 21 patients died in CR during consolidation therapy, due to infection. Event-free survival rates in patients with and without high-dose cytarabine were shown in Figure 1d.

In multivariate analysis, age and white blood cell count at diagnosis represented significant unfavorable predictors of overall survival. White blood cell count and lactate dehydrogenase level at diagnosis represented significant unfavorable predictors of event-free survival. (Table 2) Among 147 patients with AML (M2), presence of t(8;21) was not a significant predictor of survival (hazard ratio, 0.65; 95%CI 0.34–1.24; $P=0.19$) in multivariate analysis.

The present study demonstrated a more favorable survival rate for patients with t(8;21) AML in Japan than seen in recent studies conducted in western countries,[4,6–8] even though median age in the present study (49.5 years) was higher than those in recent studies (28–43 years).[4,6–8] Median white blood cell count and platelet count in the present study, which have been reported as predictors of survival in previous studies,[4,6–8] were consistent

Table 1 Characteristics and treatment of patients with t(8;21) AML

Variables		*Number*
Age (years)	Median, range	49.5 (18–86)
Sex	Male/female	32/14
Karyotypic abnormality[a]		
(A) t(8;21)(q22; q22) without additional karyotypic abnormality		12
(B) t(8;21)(q22; q22) with loss of sex (Y) chromosome		13
(C) t(8;21)(q22; q22) with abnormal chromosome 9		4
(D) t(8;21)(q22; q22) with ≥3 additional abnormalities		9
(E) t(8;21)(q22; q22) with loss of X chromosome		3
(F) Other karyotypic abnormalities[b]		3
White blood cell count (/μl)	Median, range	9350 (900–54 970)
Red blood cell count (10E6/μl)	Median, range	2.4 (0.6–4.0)
Hemoglobin at diagnosis (g/dl)	Median, range	8.5 (2.3–12.8)
Platelet count (10E3/μl)	Median, range	34 (6–99)
Lactate dehydrogenase level (IU/l)	Median, range	453 (162–3831)
Extramedullary involvement	Present[c]/absent	8/37
Surface antigens on leukemia cells		
CD 7	Present/absent	2/42
CD 13	Present/absent	41/3
CD 19	Present/absent	29/17
CD 33	Present/absent	35/11
CD 34	Present/absent	42/2
CD 56[d]	Present/absent	32/7
HLA-DR	Present/absent	44/2
First induction therapy[e]		
Idarubicine 12 mg/m^2 d1–3+cytarabine 100 mg/m^2 d1–7		37
Daunorubicine 50 mg/m^2 d1–5+cytarabine 100 mg/m^2 d1–7		3
Low-dose cytarabine-based chemotherapy		4
Other regimen		1
Outcomes of first induction therapy		
Complete remission		36
Complete remission not achieved		9[f]
Consolidation therapy[g]		
High-dose cytarabine-based chemotherapy		21
Courses of high-dose cytarabine (1/2/3/4)		1[h]/4/12/4
Standard cytarabine-based chemotherapy		16
Low-dose cytarabine-based chemotherapy		2
Hematopoietic stem cell transplantation		
In first complete remission (autologous/allogeneic)		3/4[i]
In other stage (autologous/allogeneic)		0/8

Abbreviation: AML, acute myeloid leukemia.
[a]Two patients were diagnosed by detection of RUNX1/MTG8 fusion gene using reverse transcription-polymerase chain reaction.
[b]Those included 46,XY, t(8;21)(q22;q22), del(11)(p11p13) (*n* = 1); 46,XY, t(7;21;8)(q22;q22;q22) (*n* = 1); 45,XY, t(8;12;21)(q22;p11;q22), del(9)(q?) (*n* = 1) and 46,XX,t(2;19)(q37;p13),t(8;21)(q22;q22) (*n* = 1).
[c]Including skin (*n* = 2), submandibular lymph nodes (*n* = 1), mediastinum (*n* = 2), cervical lymph nodes (*n* = 2), spleen (*n* = 2), submandibular lymph nodes (*n* = 1), liver (*n* = 1), lung (*n* = 1) and subcutaneous (*n* = 1).
[d]Mean fluorescence intensity of CD56 among karyotype group A-F was 68, 42, 48,83, 85 and 18%, respectively.
[e]One patient rejected chemotherapy.
[f]Five patients achieved complete remission after second course of induction therapy. Three of the remaining 4 patients died with disease progression at a median of 195 days (range, 92–243 days) after diagnosis. The final remaining patient underwent allogeneic peripheral blood stem cell transplantation from an HLA-matched sibling at day 114 after diagnosis.
[g]One patient did not receive consolidation therapy and data were unavailable for one patient.
[h]This patient received autologous hematopoietic stem cell transplantation in first complete remission.
[i]Those patients had received standard-dose cytarabine (*n* = 2) or high-dose cytarabine (*n* = 2) containing consolidation therapies before transplantation.

with those in previous studies. Differences in patient backgrounds between recent studies and ours are thus unlikely to have affected survival rates. These results indicate that t(8;21) AML in Japanese patients is associated with more favorable outcomes than seen in patients from western countries. Prognosis of t(8;21) AML may differ according to ethnicity, although statically analysis was not conducted. Further large-scale studies to investigate differences in clinical outcome among patients of various ethnicities thus appear warranted.

Interestingly, differences in overall survival between t(8;21) AML patients and AML(M2) without t(8;21) patients were unclear after adjusting for age (Figure 1b). One possible explanation is that AML (M2) in Japanese patients is associated with favorable outcomes. Another explanation is that favorable outcomes for t(8;21) AML are greatly related to low patient age. To date, information on clinical differences after adjusting for age between t(8;21) AML and AML(M2) without t(8;21) limited, and is worth investigating in future studies.

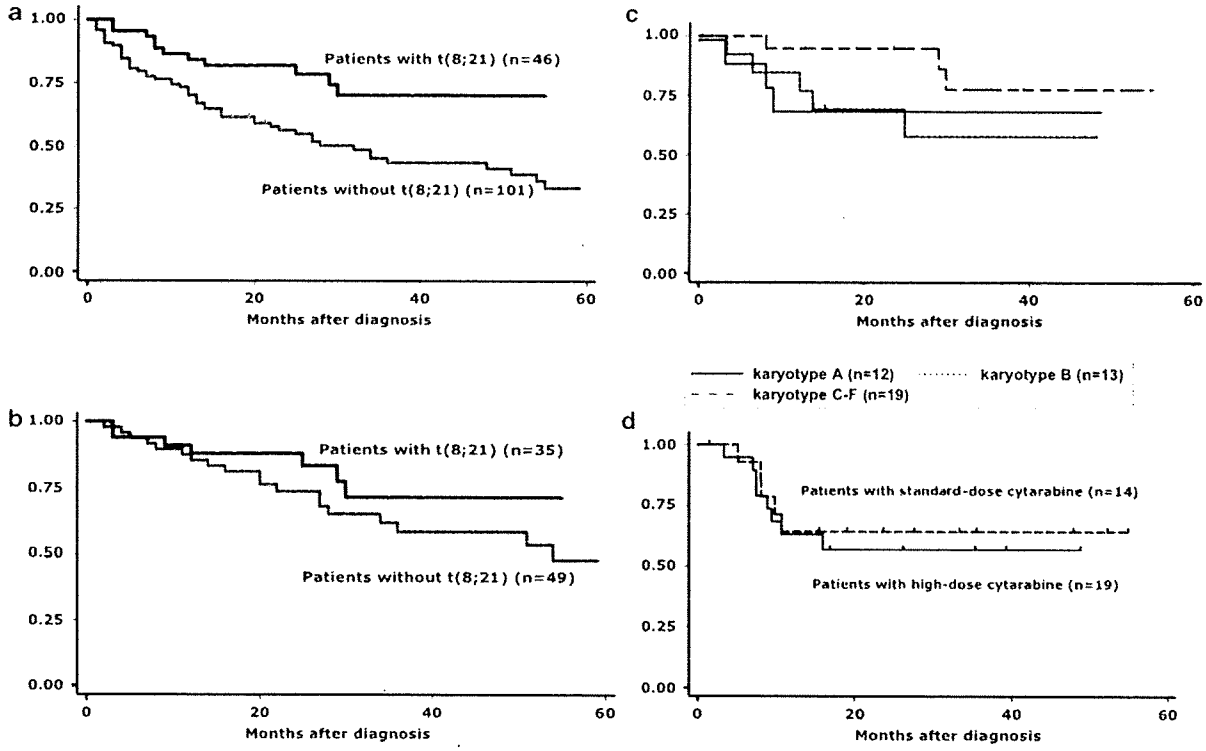

Figure 1 Overall survival rates. Overall survival rates of the AML (M2) patient with or without t(8;21) were shown in (**a**). Overall survival rate at 3 years after diagnosis in patients with t(8;21) was 0.70 (95%CI, 0.51–0.83). Overall survival rate at 3 years after diagnosis in patients with non-t(8;21) AML (M2) was 0.43 (95%CI, 0.32–0.54) (**a**). A significant difference was identified between groups (log-rank test, $P = 0.005$). Overall survival rates for AML (M2) patients <60-years-old were shown in (**b**). Overall survival rate at 3 years after diagnosis in patients with or without t(8;21) was 0.71 (95%CI, 0.47–0.86) and 0.58 (95%CI, 0.41–0.72), respectively. No significant difference was seen between groups (log-rank test, $P = 0.28$) (**b**). Overall survival rates according to karyotype at diagnosis were shown in Panel c. Survival rates of the following karyotype groups are shown: (A) t(8;21)(q22;q22) without other karyotype abnormality; (B) t(8;21)(q22;q22) with loss of sex (Y) chromosome; (C) t(8;21)(q22;q22) with abnormal chromosome 9; D) t(8;21)(q22;q22) with ⩾3 additional abnormalities; E) t(8;21)(q22;q22) with loss of X chromosome and F) other karyotype abnormalities. No significant difference was noted between groups (log-rank test, $P = 0.27$) (**c**). Event-free survival rates with high- and standard-dose cytarabine were shown in (**d**). Event-free survival rates at 3 years after diagnosis in patients with consolidation therapy containing high- and standard-dose cytarabine were 57% (95%CI, 32–76%) and 64% (95%CI, 34–83%), respectively (log-rank test, $P = 0.69$) The four patients who received the allogeneic stem cell transplantation in the first complete remission were excluded from the analysis (**d**). AML, acute myeloid leukemia; CI, confidence interval.

Table 2 Risk factors for overall and event-free survival in patients with t(8;21) AML

Univariate factors	*Overall survival*			*Event-free survival*		
	HR	*95% CI*	*P*	*HR*	*95% CI*	*P*
Age (years)	1.04	1.00–1.08	0.08	1.01	0.98–1.05	0.37
Sex (male vs female)	2.25	0.48–10.4	0.30	1.75	0.58–5.32	0.32
Induction therapies (low-dose vs standard-dose cytarabine-containing regimens)	2.57	0.55–12.0	0.23	2.65	0.76–9.23	0.13
White blood cell count at diagnosis (⩾10E4/μl vs <10E4/μl)	6.78	1.48–31.0	0.01	4.41	1.57–12.41	0.005
Hemoglobin at diagnosis (linear by 1 g/dl increase)	1.01	0.81–1.25	0.94	1.08	0.90–1.30	0.40
Platelet count at diagnosis (linear by 10E4/μl increase)	1.06	0.86–1.32	0.58	1.01	0.84–1.22	0.91
Lactate dehydrogenase level at diagnosis (linear by 1 IU increase)	1.00	1.000–1.001	0.06	1.001	1.0002–1.0011	0.004
CD56 expression of leukemia cell (positive vs negative)[a]	0.59	0.15–2.39	0.46	0.78	0.22–2.78	0.71
Karyotype (t(8:21) with other additional abnormality vs t(8;21) without additional abnormality or t(8:21) with loss of sex (Y) chromosome)[a]	1.01	0.31–3.31	0.99	1.05	0.42–2.66	0.91
Extramedullary involvement (present vs absent)	0.92	0.20–4.25	0.91	0.87	0.25–3.02	0.83
Stepwise multivariate factors						
Age (years)	1.04	1.00–1.09	0.04	NA	NA	NA
White blood cell count at diagnosis (⩾10E4/μl vs <10E4/μl)	7.70	1.66–35.7	0.009	3.68	1.29–10.50	0.02
Lactate dehydrogenase level at diagnosis (linear by 1 IU increase)	NA	NA	NA	1.001	1.000–1.001	0.02

Abbreviations: AML, acute myeloid leukemia; 95% CI, 95% confidence interval; HR, hazard ratio; NA, not applicable.
[a]Patients with an unknown variable were included in the analysis using a dummy variable indicating missing data.

Additional karyotype abnormalities have been reported as an unfavorable prognostic factor for t(8;21) AML.[1] The significance of these abnormalities may vary with ethnicity.[4] In the present study, the prognostic impact of additional karyotype abnormalities (including loss of the sex chromosome and abnormal chromosome 9) was uncertain, consistent with a previous study from Japan.[5] Additional karyotype abnormalities may not represent an important prognostic factor in Japanese patients. However, trisomy 4 still requires special consideration. All 3 Japanese patients with trisomy 4 in an earlier study died within 3 years.[5] This additional karyotype warrants further investigation, since the present study did not include these patients.

No clinical impact of high-dose cytarabine consolidation therapy in Japanese t(8;21) AML patients was demonstrated in the present study, inconsistent with previous studies from western countries.[1,2] Efficacy of high-dose cytarabine may differ between patients from Japan and western countries. Since intensive chemotherapy such as high-dose cytarabine carries a risk of treatment-related morbidity and mortality, clinicians must carefully select eligible patients who would benefit from this regimen. Overall survival rate in patients with high-dose cytarabine was not inferior to that in patients who received standard or low-dose regimens (data not shown). Our results indicate that high-dose cytarabine consolidation chemotherapy is feasible in Japanese patients with t(8;21) AML and that investigation of efficacy by conducting a randomized trial in Japan is warranted.

Despite providing novel and useful information on t(8;21) AML in Japan, some issues remain to be discussed. First, the patients known to have a less good prognosis, such as those with additional trisomy 4 was not included in the present study. Second, the information on tyrosine kinase mutations in the patients with t(8;21) was not presented in the present study. The tyrosine kinase mutations among various ethnicities are require to investigate in future studies, since those could influence the prognosis. Furthermore, specific mutations often associated with t(8;21), such as N-Ras and Flt3 besides c-kit are also worth investigating. The last detailed information of AML(M2) patients without t(8;21), including white blood cell count and karyotype at diagnosis, and induction and consolidation treatment were not available in the present study. Those require to be investigated in future studies.

In summary, the clinical characteristics of t(8;21) AML might differ between patients from Japan and western countries. Clinicians should be alert to potential clinical differences among ethnicities. Further large-scale studies on differences in clinical characteristics among various ethnicities including Japanese patients are required.

Acknowledgements

We thank all the staff and resident members of the participating institutions. A complete list of participating institutions appears in the Appendix.

H Narimatsu[1,2], T Yokozawa[3], H Iida[4], M Tsuzuki[5], M Hayakawa[6], T Takeo[7], M Iino[8], T Ichihashi[9], C Kato[5], A Sawamoto[1], H Sao[4], M Yanada[2], N Emi[5], H kiyoi[10], T Yamaguchi[9], T Naoe[2], R Suzuki[11] and I Sugiura[1]

[1]*Department of Hematology and Oncology, Toyohashi Municipal Hospital, Toyohashi, Japan;*
[2]*Department of Hematology and Oncology, Nagoya University Graduate School of Medicine, Nagoya, Japan;*
[3]*Department of Hematology/Oncology, Clinical Research Center, National Hospital Organization Nagoya Medical Center, Nagoya, Japan;*
[4]*Department of Hematology, Meitetsu Hospital, Nagoya, Japan;*
[5]*Department of Medicine, Fujita Health University School of Medicine, Toyoake, Japan;*
[6]*Department of Hematology, Komaki City Hospital, Komaki, Japan;*
[7]*Department of Hematology, Yokkaichi Municipal Hospital, Yokkaichi, Japan;*
[8]*Department of Hematology, Yamanashi Prefectual Central Hospital, Kofu, Japan;*
[9]*Department of Hematology, Okazaki City Hospital, Okazaki, Japan;*
[10]*Department of Infectious Diseases, Nagoya University School of Medicine, Nagoya, Japan and*
[11]*Department of HSCT Data Management, Nagoya University School of Medicine, Nagoya, Japan*
E-mail: narimt54@med.nagoya-u.ac.jp

References

1 Ferrara F, Del Vecchio L. Acute myeloid leukemia with t(8;21)/AML1/ETO: a distinct biological and clinical entity. *Haematologica* 2002; **87**: 306–319.
2 Byrd JC, Dodge RK, Carroll A, Baer MR, Edwards C, Stamberg J *et al.* Patients with t(8;21)(q22;q22) and acute myeloid leukemia have superior failure-free and overall survival when repetitive cycles of high-dose cytarabine are administered. *J Clin Oncol* 1999; **17**: 1767–3775.
3 Grimwade D, Walker H, Oliver F, Wheatley K, Harrison C, Harrison G *et al.* The importance of diagnostic cytogenetics on outcome in AML: analysis of 1612 patients entered into the MRC AML 10 trial. The Medical Research Council Adult and Children's Leukaemia Working Parties. *Blood* 1998; **92**: 2322–2333.
4 Marcucci G, Mrozek K, Ruppert AS, Maharry K, Kolitz JE, Moore JO *et al.* Prognostic factors and outcome of core binding factor acute myeloid leukemia patients with t(8;21) differ from those of patients with inv(16): a Cancer and Leukemia Group B study. *J Clin Oncol* 2005; **23**: 5705–5717.
5 Nishii K, Usui E, Katayama N, F Lorenzo V, Nakase K, Kobayashi T *et al.* Characteristics of t(8;21) acute myeloid leukemia (AML) with additional chromosomal abnormality: concomitant trisomy 4 may constitute a distinctive subtype of t(8;21) AML. *Leukemia* 2003; **17**: 731–737.
6 Nguyen S, Leblanc T, Fenaux P, Witz F, Blaise D, Pigneux A *et al.* A white blood cell index as the main prognostic factor in t(8;21) acute myeloid leukemia (AML): a survey of 161 cases from the French AML Intergroup. *Blood* 2002; **99**: 3517–3523.
7 Schlenk RF, Benner A, Krauter J, Buchner T, Sauerland C, Ehninger G *et al.* Individual patient data-based meta-analysis of patients aged 16 to 60 years with core binding factor acute myeloid leukemia: a survey of the German Acute Myeloid Leukemia Intergroup. *J Clin Oncol* 2004; **22**: 3741–3750.
8 Appelbaum FR, Kopecky KJ, Tallman MS, Slovak ML, Gundacker HM, Kim HT *et al.* The clinical spectrum of adult acute myeloid leukaemia associated with core binding factor translocations. *Br J Haematol* 2006; **135**: 165–173.

Appendix

This study was conducted at the following institutions: National Hospital Organization Nagoya Medical Center, Nagoya; Toyohashi Municipal Hospital, Toyohashi; Meitetsu Hospital, Nagoya; Fujita Health University Hospital, Toyoake; Komaki City Hospital, Komaki; Yokkaichi Municipal Hospital, Yokkaichi; Yamanashi Prefectural Central Hospital, Yamanashi; Okazaki City Hospital, Okazaki, Japan.

MOLECULAR AND CELLULAR BIOLOGY, Apr. 2008, p. 2125–2137 Vol. 28, No. 7
0270-7306/08/$08.00+0 doi:10.1128/MCB.00740-07

Inducible Expression of Chimeric EWS/ETS Proteins Confers Ewing's Family Tumor-Like Phenotypes to Human Mesenchymal Progenitor Cells▽†

Yoshitaka Miyagawa,[1] Hajime Okita,[1]* Hideki Nakaijima,[1] Yasuomi Horiuchi,[1] Ban Sato,[1] Tomoko Taguchi,[1] Masashi Toyoda,[3] Yohko U. Katagiri,[1] Junichiro Fujimoto,[2] Jun-ichi Hata,[1] Akihiro Umezawa,[3] and Nobutaka Kiyokawa[1]

Department of Developmental Biology, National Research Institute for Child Health and Development, 2-10-1, Okura, Setagaya-ku, Tokyo 157-8535, Japan[1]; National Research Institute for Child Health and Development, 2-10-1, Okura, Setagaya-ku, Tokyo 157-8535, Japan[2]; and Department of Reproductive Biology, National Research Institute for Child Health and Development, 2-10-1, Okura, Setagaya-ku, Tokyo 157-8535, Japan[3]

Received 27 April 2007/Returned for modification 13 July 2007/Accepted 7 January 2008

Ewing's family tumor (EFT) is a rare pediatric tumor of unclear origin that occurs in bone and soft tissue. Specific chromosomal translocations found in EFT cause EWS to fuse to a subset of ets transcription factor genes (ETS), generating chimeric EWS/ETS proteins. These proteins are believed to play a crucial role in the onset and progression of EFT. However, the mechanisms responsible for the EWS/ETS-mediated onset remain unclear. Here we report the establishment of a tetracycline-controlled EWS/ETS-inducible system in human bone marrow-derived mesenchymal progenitor cells (MPCs). Ectopic expression of both EWS/FLI1 and EWS/ERG proteins resulted in a dramatic change of morphology, i.e., from a mesenchymal spindle shape to a small round-to-polygonal cell, one of the characteristics of EFT. EWS/ETS also induced immunophenotypic changes in MPCs, including the disappearance of the mesenchyme-positive markers CD10 and CD13 and the up-regulation of the EFT-positive markers CD54, CD99, CD117, and CD271. Furthermore, a prominent shift from the gene expression profile of MPCs to that of EFT was observed in the presence of EWS/ETS. Together with the observation that EWS/ETS enhances the ability of cells to invade Matrigel, these results suggest that EWS/ETS proteins contribute to alterations of cellular features and confer an EFT-like phenotype to human MPCs.

Ewing's family tumor (EFT) is a rare childhood cancer arising mainly in bone and soft tissue. Since EFT has a poor prognosis, it is important to elucidate the underlying pathogenic mechanisms for establishing a more effective therapeutic strategy. EFT is characterized by the presence of chimeric genes composed of EWS and ets transcription factor genes (ETS) formed by specific chromosomal translocations, i.e., EWS/FLI1, t(11;22)(q24;q12); EWS/ERG, t(21;22)(q12;q12); EWS/ETV1, t(7;22)(p22;q12); EWS/E1AF, t(17;22)(q12;q12); and EWS/FEV, t(2;22)(q33;q12) (26). The products of these chimeric genes behave as aberrant transcriptional regulators and are believed to play a crucial role in the onset and progression of EFT (3, 36). Indeed, recent studies have revealed that the induction of EWS/FLI1 proteins can trigger transformation in certain cell types, including NIH 3T3 cells (36), C2C12 myoblasts (12), and murine primary bone marrow-derived mesenchymal progenitor cells (MPCs) (6, 45, 52). However, studies have also indicated that overexpression of EWS/FLI1 provokes apoptosis and growth arrest in mouse normal embryonic fibroblasts and primary human fibroblasts (10, 31), hence hampering understanding of the precise role of EWS/ETS proteins in the development of EFT. The function of EWS/ETS proteins would be greatly influenced by cell type, and thus the cells that can originate EFTs might be more susceptible to the tumorigenic effects of EWS/ETS.

Although the cell origin of EFT is still unknown, the expression of neuronal markers in spite of the occurrence in bone and soft tissues has kept open the debate as to a potential mesenchymal or neuroectodermal origin. As described above, ectopic expression of EWS/FLI1 results in dramatic changes in morphology and the formation of EFT-like tumors in murine primary bone marrow-derived MPCs but not in murine embryonic stem cells (6, 45, 52), supporting the notion that MPCs are a plausible cell origin of EFT (45). However, others argue that MPCs cannot be considered progenitors of EFT without further evidence of similarity between human EFT and MPC-EWS/FLI1-induced tumors in mice (29, 46).

The development of experimental systems using murine species is useful for elucidating the mechanisms behind the pathogenesis of EFT. However, several differences between human and murine systems cannot be ignored; these differences include the expression patterns of surface antigens in MPCs, for instance (7, 44, 51, 53). Moreover, human cells are difficult to transform in vitro, and the transformed cells of mice seem to produce a more aggressive tumor than those of hu-

* Corresponding author. Mailing address: Department of Developmental Biology, National Research Institute for Child Health and Development, 2-10-1, Okura, Setagaya-ku, Tokyo 157-8535, Japan. Phone: 81-3-3416-0181. Fax: 81-3-3417-2496. E-mail: okita@nch.go.jp.

† Supplemental material for this article may be found at http://mcb.asm.org/.

▽ Published ahead of print on 22 January 2008.

TABLE 1. Cell lines used in this study and fusion transcript types

Cell line	Diagnosis	Fusion transcript type	Reference
EES-1	EFT	EWS/FLI1 type I	20
SCCH196	EFT	EWS/FLI1 type I	21
RD-ES	EFT	EWS/FLI1 type II	5
SK-ES1	EFT	EWS/FLI1 type II	5
NCR-EW2	EFT	EWS/FLI1 type II	19
NCR-EW3	EFT	EWS/E1AF	19
W-ES	EFT	EWS/ERG	13
NB69	NB		15
NB9	NB		15
GOTO	NB		47
NRS-1	RMS	PAX3/FKHR	40

mans (1). The findings suggest the existence of undefined cell-autonomous mechanisms that render human cells resistant to malignant transformation. Therefore, the use of human cell models is ideal for clarifying how EFT develops. Models of the onset of EFT have been generated using primary fibroblasts (31) and rhabdomyosarcoma cells (23). However, these cell types are not appropriate for studying the origins of EFT, and a model that precisely recapitulates EWS/ETS-mediated EFT formation is required.

UET-13 cells are obtained by prolonging the life span of human bone marrow stromal cells by use of the retroviral transgenes hTERT and E7 (38, 50), retain the ability to differentiate into not only mesodermal derivatives but also neuronal progenitor-like cells, and are considered a good model for studying the cellular events in human MPCs. Therefore, we have examined the biological effect of EWS/ETS in human MPCs by use of UET-13 cells by exploiting tetracycline-inducible systems for expressing EWS/ETS (EWS/FLI1 and EWS/ERG). Here we report that overexpression of EWS/ETS mediates an EFT-like phenotype, including morphology, immunophenotype, and gene expression profile, with enhancement of the Matrigel invasion ability of UET-13 cells.

MATERIALS AND METHODS

Cell cultures and establishment of UET-13TR-EWS/ETS cell lines. UET-13 cells were cultured in Dulbecco's modified Eagle's medium (DMEM) with 10% Tet system approved fetal bovine serum (T-FBS) (Takara) at 37°C under a humidified 5% CO_2 atmosphere. EFT cell lines (EES-1 [20], SCCH196 [21], RD-ES and SK-ES1 [5], NCR-EW2 and NCR-EW3 [19], and W-ES [13]) and neuroblastoma (NB) cell lines (NB69 and NB9 [15] and GOTO [47]) were cultured in RPMI 1640 with 10% FBS. A rhabdomyosarcoma cell line, NRS-1 (40), was cultured in Eagle's minimal essential medium with 10% FBS. The cell lines used in this study are listed in Table 1.

UET-13 cells were seeded at a density of 5×10^4 cells per well in 24-well tissue culture plates 1 day prior to transfection. For introducing the tetracycline-inducible system, UET-13 cells were transfected with pcDNA6-TR (Invitrogen) by use of Lipofectamine 2000 (Invitrogen). After 72 h, the medium was replaced with fresh medium containing 200 μg/ml of blasticidin S (Invitrogen). Individual resistant clones were selected for a month and designated UET-13TR cells. UET-13TR cells were further transfected with pcDNA4-EWS/ETSs constructed as described below, and individual resistant clones were selected in DMEM containing 10% T-FBS and 200 to 300 μg/ml of Zeocin (Invitrogen). The Zeocin-resistant clones were expanded and tested for the induction of EWS/ETS expression upon the addition of tetracycline by use of reverse transcription-PCR (RT-PCR) as described below.

Plasmid construction. A gateway cassette (bases 1 to 1705) was amplified from pBLOCK-iT3-DEST (Invitrogen) by PCR, and the PCR product was inserted into the EcoRV site of pcDNA4-TO (Invitrogen) (termed pcDNA4-DEST). Since the type II EWS/FLI1 is a stronger transactivator than the type I product (32), we used the type II variant in the present study. EWS/ERG was isolated from W-ES, an EFT cell line, joining EWS exon 7 and ERG exon 9. Full-length EWS/FLI1 type II and EWS/ERG cDNAs were amplified from cDNAs prepared from NCR-EW2 and W-ES cells, respectively, by PCR as described below and cloned into the XmnI-EcoRV sites of pENTR11 (Invitrogen). The resulting pENTR11-EWS/ETSs were recombined with pcDNA4-DEST by use of LR recombination reaction as instructed by the manufacturer (Invitrogen) to construct the tetracycline-inducible EWS/ETS expression vector pcDNA4-EWS/ETSs.

Western blot analysis. UET-13 transfectants were cultivated with or without 3 μg/ml of tetracycline for 72 h. Western blot analysis was performed as previously described (37). Briefly, the cell lysates were prepared and separated on a 10% sodium dodecyl sulfate-polyacrylamide gel electrophoresis gel and transferred onto a polyvinylidene difluoride membrane. The membranes were blocked with 5% skimmed milk in phosphate-buffered saline (PBS) containing 0.01% Tween 20 (Sigma) and incubated with primary antibodies. As the primary antibodies, anti-Fli-1, anti-Erg-1/2/3 (Santa Cruz Biotechnology), and anti-actin (Sigma) were used. Horseradish peroxidase-conjugated anti-rabbit or anti-mouse immunoglobulin G (IgG) antibodies (DakoCytomation) were used as secondary antibodies. Blots were detected by chemiluminescence using an ECL Plus Western blotting detection system (GE Healthcare Bio-Science Corp.) and exposed to X-ray film (Kodak) for 5 to 30 min.

MTT assay and detection of apoptosis. Growth curves of UET-13 transfectants were determined using the 3-(4,5-dimethylthiazol-2-yl)-2,5-diphenyltetrazolium bromide (MTT) assay as described previously (18). The apoptosis was detected using an annexin V-fluorescein isothiocyanate (FITC) apoptosis detection kit (Biovision) according to the manufacturer's instructions and analyzed by flow cytometry (Cytomics FC500; Beckman Coulter).

Immunofluorescence analysis. After 1 week of culture in the absence or presence of tetracycline, UET-13 cells and the transfectants were harvested with 0.25% trypsin plus EDTA (IBL). The cells (2×10^5) were incubated with mouse monoclonal antibodies for 20 min. In the case of fluorescence-labeled antibodies, the cells were washed with PBS and then analyzed. In the case of primary unconjugated mouse antibodies, the cells were washed and then incubated with FITC-conjugated goat anti-mouse IgG antibody (Jackson ImmunoResearch Laboratories) for 20 min. Cell fluorescence was detected using a Cytomics FC500 instrument as described previously (27).

Antibodies against the following human antigens were used: CD10, CD13, CD14, CD29, CD34, CD40, CD44, CD45, CD49e, CD54, CD56, CD61, CD90, CD105, CD117, and CD166 from Beckman Coulter; CD73 from BD Biosciences-Pharmingen; CD55 from Abcam; CD59 from Cedarlane Laboratories; and CD133 and CD271 from Miltenyi Biotec GmbH.

Immunocytochemistry. Cells were grown on collagen type I-coated cover glasses (Iwaki). After 72 h with or without tetracycline, cells were fixed for 30 min in 4% paraformaldehyde and permeabilized in PBS containing 0.2% Triton X-100 (Sigma) for 30 min. Subsequently, they were washed with PBS and blocked in PBS containing 0.1% Triton X-100 and 1% bovine serum albumin (Sigma) for 30 min before being incubated with a monoclonal anti-CD99 antibody, i.e., 12E7 (1:100) (DakoCytomation) or O13 (1:200) (Thermo), and polyclonal anti-Fli-1 antibody (1:100) (Santa Cruz) for 1 h. Bound antibodies were visualized with appropriate secondary antibodies, i.e., Alexa Fluor 488 goat anti-mouse IgG (heavy plus light chains) highly cross-adsorbed and Alexa Fluor 546 goat anti-rabbit IgG (heavy plus light chains) highly cross-adsorbed (Invitrogen) for 1 h at 1:300. Nuclei were counterstained with 4′,6′-diamidino-2-phenylindole (DAPI) or propidium iodide (PI) (Sigma). For the visualization of whole cells, cells were treated with Celltracker Blue (Invitrogen) for 30 min and then fixed. Fluorescence was observed and analyzed using a confocal laser scanning microscope and image software (either FV500 from Olympus or LSM510 from Carl Zeiss). Precise measurements of cell size, nuclear size, and the nucleus-to-cytoplasm (N/C) ratio were performed using Image J (16).

RT-PCR analysis. Total RNA was extracted from cells by use of an RNeasy kit (Qiagen) and reverse transcribed using a first-strand cDNA synthesis kit (GE Healthcare Bio-Science Corp). RT-PCR was performed with a HotstarTaq master mix kit (Qiagen). As an internal control, human GAPDH cDNA was also amplified. The sequences of gene-specific primers for RT-PCR were as follows: for EWS/FLI1 (forward), 5′-ATGGCGTCCACGGATTACAGTACCT-3′; for EWS/FLI1 (reverse), 5′-GGGTCTTCTTTGACACTCAATCG-3′; for EWS/ERG (forward), 5′-ATGGCGTCCACGGATTACAGTACCT-3′; for EWS/ERG (reverse), 5′-TTAGTAGTAAGTGCCCAGATGAGAA-3′; for GAPDH (forward), 5′-CCACCCATGGCAAATTCCATGGCA-3′; and for GAPDH (reverse), 5′-TCTAGACGGCAGGTCAGGT/CCACC-3′. PCR products were electrophoresed with a 1% agarose gel and stained with ethidium bromide.

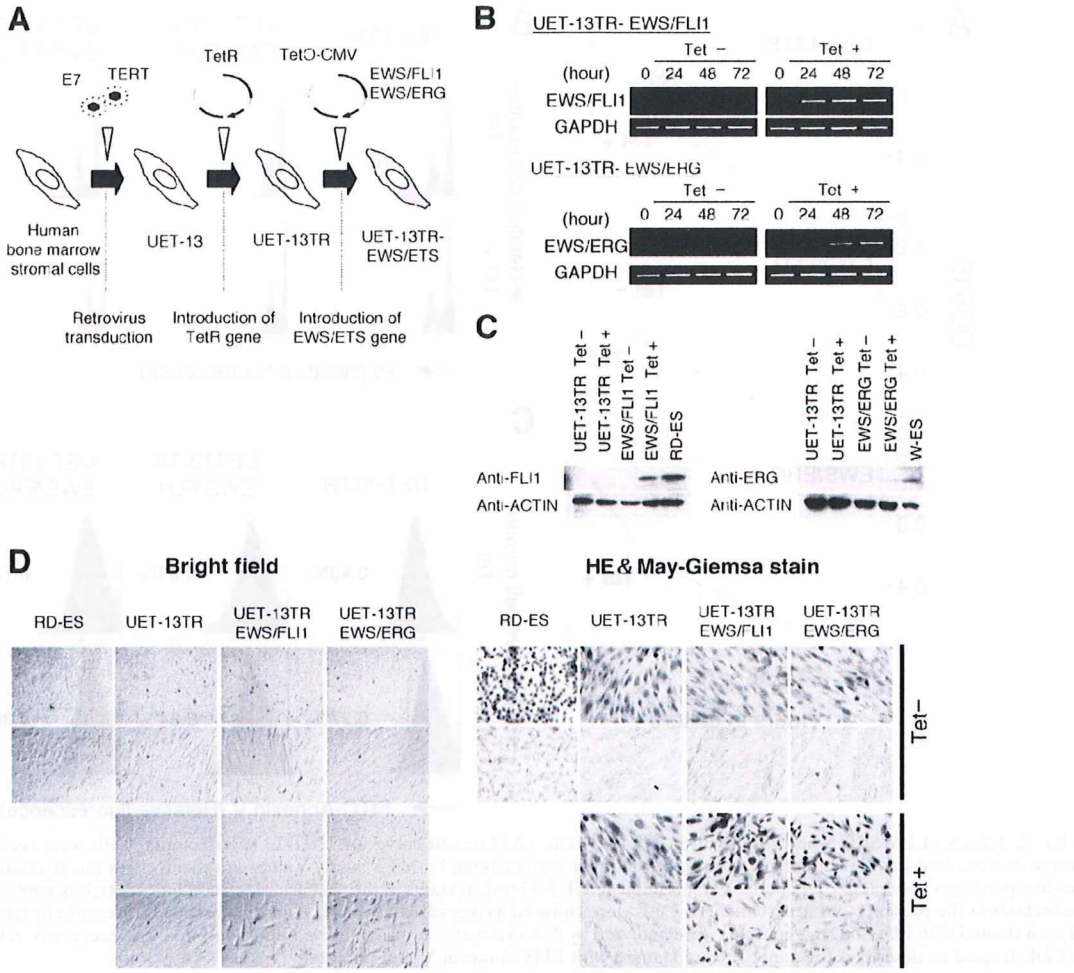

FIG. 1. The effect of EWS/ETS on the morphology of UET-13 cells. (A) The establishment of a tetracycline-inducible EWS/ETS expression system in UET-13 cells. CMV, cytomegalovirus. (B) Analyses for confirming the inducible expression of EWS/ETS genes. EWS/ETS mRNAs were detected in UET-13 transfectants UET-13TR-EWS/FLI1 and UET-13TR-EWS/ERG by RT-PCR. These cells were treated with or without 3 μg/ml of tetracycline (Tet) for the indicated periods. As an internal control, a human GAPDH gene was used. (C) Analyses for confirming the inducible expression of EWS/ETS proteins. The cells were treated as described for panel B and subjected to Western blotting for the detection of EWS/ETS proteins. The extracts of RD-ES and W-ES cells were also examined as positive controls. Membranes were reprobed with anti-actin antibody as a loading control. (D) Morphological change after tetracycline treatment of UET-13 transfectants. UET-13 cells and the transfectants were cultured in the absence or presence of tetracycline for 72 h and observed by light microscopy. Magnification, ×40 (top); ×200 (bottom). Cells were also examined using hematoxylin-eosin (HE) (top) and May-Giemsa (bottom) staining (magnification, ×200).

Real-time RT-PCR. Real-time RT-PCR was performed using TaqMan universal PCR master mix and TaqMan gene expression assays and an inventoried assay on an ABI Prism 7900HT sequence detection system (Applied Biosystems) according to the manufacturer's instructions. The human GAPDH gene was used as an internal control for normalization.

DNA microarray analysis. Total RNA isolated from cells was reverse transcribed and labeled using one-cycle target labeling and control reagents as instructed by the manufacturer (Affymetrix). The labeled probes were hybridized to the human genome U133 Plus 2.0 array (Affymetrix). The arrays were performed in a single experiment and analyzed using GeneChip operating software, version 1.2 (Affymetrix). Background subtraction, normalization, and principal component analysis (PCA) were performed by GeneSpring GX 7.3 software (Agilent Technologies). Signal intensities were prenormalized based on the median of all measurements on that chip. To account for the difference in detection efficiencies between the spots, prenormalized signal intensities on each gene were normalized to the median of prenormalized measurements for that gene. The data were filtered using the following steps. (i) Genes that were scored as absent in all samples were eliminated. (ii) Genes for which the signal intensities were lower than 100 were eliminated. (iii) Performing cluster analysis using filtering genes, we selected the genes that exhibited increased expression or decreased expression in tetracycline-treated cells. Accession numbers for the microarray data are given below.

Invasion assay. The invasion assay was performed using Matrigel (BD Bioscience) according to the previous description (34) with some modification. Polycarbonate filter inserts containing 8-μm pores (BD Falcon) were coated with 50 μl of a 6:1 mixture of culture medium and Matrigel and placed into 24-well culture plates containing DMEM supplemented with 10% T-FBS as chemoattractants. Cells (2.5×10^4) treated with or without tetracycline for 72 h were suspended in DMEM containing 0.01% T-FBS and plated on top of each filter insert. After 20 h in culture in the presence or absence of tetracycline, noninvading cells were removed from upper surface of the filter with a cotton swab. The invading cells on the lower surface of the filter were fixed with formalin, stained with hematoxylin-eosin, and counted in five fields per membrane with light microscopy. As a control, cells were also cultured on uncoated filter inserts. The invasion efficiency was presented as the ratio of the number of invading cells on Matrigel-coated inserts to that on uncoated inserts. Experiments were performed in triplicate, and the means with standard deviations of the values are shown in the graphs in Fig. 8.